Development of New Type of High Power RF Windows

Sergey Kazakov

Doctor of Philosophy

Department of Accelerator Science
School of Mathematical and Physical Science
The Graduate University for Advanced Studies

February 2003

Abstract

The design and results of cold and high power measurements of several new types of windows are described in this thesis. All windows are based on the principle of traveling wave in the ceramic region. This approach allows reducing drastically the strength of electric field in the ceramic region and increasing the maximum power that can be transmitted through a window without breakdown.

A S-band traveling-wave window at 2856 MHz was design and tested. The high power testing results showed that more than 450 MW power with 2μs pulse length at 50pps repetition rate was transmitted through the window without destruction.

A X-band mixed-mode window with low electric field at the ceramic-metal brazing area was designed, and several of them were manufactured and are being used in PPM klystrons for a linear collider. Those windows are compact, though being wideband and powerful. The transmission of more than 80 MW power was achieved with 1.5μs pulse length at 30pps repetition rate.

A X-band TE_{01}-TE_{02} window was also designed. This window has low electric field on the ceramic and no electric field at the ceramic-metal brazing area to be more robust for high power transmission. The window has a simple shape, and it is compact and wideband. A low power model was manufactured and measured. This window has two new types of simple TE10-TE01 mode converters on both sides. The design and the performance measurements of those converters are also described.

Contents

List of figures

List of tables

Chapter 1

1.1 Introduction

The future of high energy physics depends strongly on building an electron-positron Linier Colliders (LC) with the center of mass energy of around 1 TeV. Why do we need an electron-positron collider when a proton – antiproton machine of this range of energy exists? According to the current understanding, the proton and the antiproton are not elementary particles like leptons (electron, positron, muons) and consist of elementary particles – three quarks. Thus the energy per particles becomes smaller and the analysis of interaction is extremely complicated. To get lucid results, real elementary particles such as electrons have to be accelerated. Future colliders must be linear because electrons are light and the energy of 1 TeV corresponds to a large relativistic factor. The power of synchrotron radiation in cyclic accelerators is proportional to the fourth power of the relativistic factor and is inversely proportional to the square of orbit radius. In 1 TeV range, a circular electron-positron collider is beyond man's capability because of large radiation losses. Particles in a linear accelerator have no synchrotron radiation and linear colliders are indispensable hopes of high energy physics now. Several main acceleration laboratories in the world are working for LC projects. These projects have many very difficult tasks. One of them is developing of RF power sources. The length of future LC and its cost depend on the achievable accelerating gradient. It was found experimentally that an accelerating gradient close to 100 MV/m could be obtained with copper structure. Choosing the wavelength, we can estimate the storage energy and the required pulse power. The power is approximately proportional to the square of wavelength. At the same time, building of RF sources becomes more difficult as the wavelength gets shorter because of the high power density. Now, several LC project are proposed. In the 'warm' (not superconductive) projects, they have the frequency range from 3 GHz to 30 GHz. But we believe that the X–band is optimal for the modern technology. To provide the maximum accelerating gradient in X-band, the power of 100 MW/m is necessary. The most probable candidate for RF power source of LC is klystron. Several prototypes of pulsed klystron with the output power of about 75 MW were built in BINP (Russia), KEK (Japan) and SLAC (USA). The RF power source with modulator is the most expensive part of LC projects. To decrease the number of RF sources, it is necessary to use a pulse compression system such as DLDS or SLED-II. Nevertheless, a X-band linear collider will need thousands of klystrons. It concludes from this fact that the RF source must have very high reliability and long lifetime.

Otherwise, most of time will be spent for klystron replacing and repairing. That will make the operating cost enormous.

One of the crucial elements in klystron, which determents the lifetime and the reliability and limits the output power, is dielectric RF window. The window is a device, which separates the vacuum of RF sources from surroundings and allows to transmit the RF power at the same time. The main part of window is a dielectric plate brazed in a metal waveguide. The problem is that if the dielectric is destroyed by pulse or average high power, the window loses hermiticity and the RF source fails. In the case of high pulse power, the main reason of window damage is RF breakdown on the surface or in the body of dielectric, which is caused by a high electric field. The modern X-band high power klystrons have two outputs to reduce power transmitted through one window. But even in this case, the window should transmit reliably the power of about 50 MW with pulse length of 1.5 – 3 μs and at 50 – 150 pps repetition rate. We have to note, that a window must endure breakdowns in loads (accelerating structure, pulse compression system). The breakdown can cause a reflected wave, which can double the electric field on the window dielectric. The doubled field corresponds to four times of more power. It means the window should be capable of transmitting the power four times lager than the maximum power of klystron. It is not a simple task to build a X-band window with such parameters. Until recently, this range of power was typical for S-band with wavelength four times larger than in the X-band. For example, the SLAC 65 MW S-band klystron 5045 has two windows. The 100 MW Toshiba klystron E3712 has two windows and special view ports to observe the surface of window ceramic because the power is close to the window limit. The S-band window cannot be scaled to the X-band because the density of power is 16 times higher at X-band and the window will be surely destroyed. New approaches are necessary. In this work, we will describe new types of RF windows with parameters close to requirements.

1.2 Brief history

Taking into account the importance of the problem, the considerable efforts were under way for development of high power X-band windows. In the works [1-5], the dielectric materials for RF windows based on Al_2O_3 were investigated. The processes on the surface of ceramic before and after breakdown were studied. It is shown that the pure Al_2O3 ceramic is one of the best materials and its electric field limit is 8 kV/mm. A higher electric field causes breakdown and distraction of ceramic. We will use this value for estimation of the maximum RF power for window hereafter.

It was found that the surface multipactor discharge could be suppressed by coating the ceramic with TiN. The optimum thickness is 1.5 nm, which would reduce the secondary emission but not thick enough to absorb RF power sufficiently.

Many works were devoted to searching of proper geometry of window [6-13]. Attempts were started from a simple half-wave window in rectangular waveguide [6]. The power limit for this window was 11 MW at 70ns. Pillbox windows [8] and long pillbox windows [13] were also investigated. The achieved power was 30 MW at 200 ns and 50 MW at 80 ns respectively. The half-wave window with the increased diameter of ceramic and the smooth transition from rectangular waveguide to circular was developed [11]. The best result for this window was 84 MW at 700 ns. The characteristics of this and pillbox windows are described in Appendixes 3 and 2.

The appreciable step in development was made when the author offered the concept of window with travelling-wave in ceramic [10]. But before jumping to the description of this type of window, we will briefly summarize problems below, which arise during the window design.

1.3 Window problems

Volume resonsnces

The main problem of X-band RF window for LC application is large power per unit of ceramic surface, which generates a high electric field and this leads to breakdowns and window distraction. The problem seems to be solved simply by increasing the size of ceramic. However, the window input and output must be single-mode waveguides as a rule. If the diameter of window is lager then 0.77 times the wavelengths, the high quality factor resonances can appear in the volume. These resonances have to be far from the operating frequency. Otherwise, even a small coupling with a resonance can entail high fields and breakdowns. The reason of coupling can be a slight asymmetry of geometry due to non-perfect manufacturing. The volume of window grows with the ceramic size, especially if a smooth taper from single mode waveguide to ceramic is used. The density of resonances increases with growth of volume too. For example, let us take a typical window from [11]. The window has a half-wave 51 mm thick ceramic and smooth taper transitions from the rectangular waveguides to the ceramic diameter. More detailed characteristic of this window is described in Appendix 3. Figure 1.2.1 shows the spectrum of volume resonances. We can see that the average distance between the resonances is

about 100 MHz. The maximum of electric field is 9.2 kV/mm for 100 MW. To decrease the field by 1.5 times, we should increase the ceramic size, and as the results, the volume size increases by 3.3 times. It results in the average resonance distance of 30 MHz. For the window with the required 100 MHz passband, this is not acceptable.

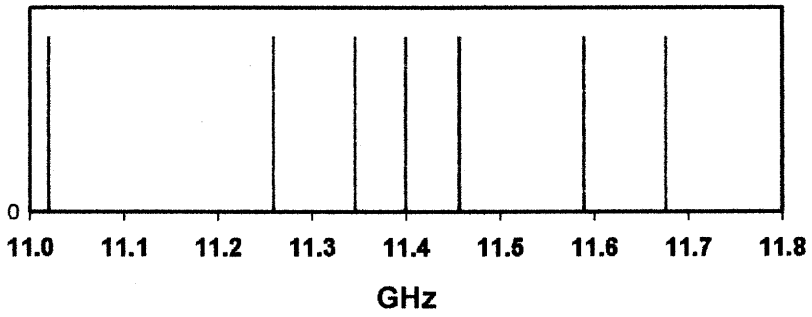

Figure 1.3.1: Volume resonances of 51 mm half-wave window with taper transitions

Ghost-modes

Another problem, due to a large size of window, is the high density of ceramic resonances, so called 'ghost modes'. The permittivity of ceramic is more than one (the permittivity of Al_2O_3 ceramic is about 9.8). The cut off wavelengths of some modes are larger in waveguide with dielectric than without it. Some modes can propagate in the ceramic disk but cannot do so in the vacuum part. Thus, the ceramic disk in waveguide works as a closed volume, which has its own resonances. The equations for resonant frequencies are written in Appendix 1. For example, Figure 1.3.2 presents ghost mode frequencies of the window mentioned above. We can see that the average distance between ghost modes are about 75 MHz and a further size increase will not be easy.

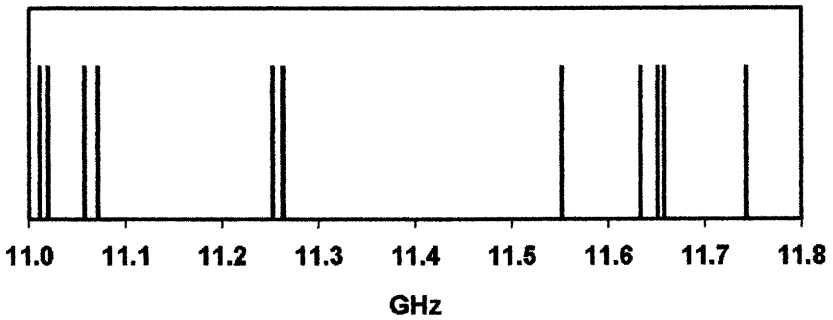

Figure 1.3.2: Ghost modes of 51 mm half-wave window with taper transitions

Passband

The important characteristic of window is the passband, which should be taken into account during the design. A large size of window leads to a narrow band as rule. But the narrow band will distort pulse and decrease the efficiency. The narrow band also will make the tolerance of dimension tighter.

Electric field in the ceramic-metal brazing area

As experiences show, the weakest place of window is the ceramic-metal brazing area. Because the ceramic metallization and brazing are not perfect, the breakdown can happen at even lower electric field. The window destruction begins often from the periphery of the ceramic. Therefore, not only the maximum electric field on the ceramic, but real field distribution should be considered during the design process.

1.4 Goals of the work

And now we can formulate the main goal of this work:

To develop a X-band window, which can be used in RF sources for future Linier Collides with output power range of 100 MW.

To reach goal, we have to:

Try to find theoretically the way to decrease the fields on/in the dielectric and increase window power, keeping in mind all above-mentioned problems;

Make a cold and high power models and to test them checking the founded solutions;

Chapter 2

Window with travelling-wave in dielectric

2.1 Trwvelling-wave window – definition and properties

We shall start the description of principle of window with travelling-wave in dielectric from the analyses of half-wave window. As an example of half-wave window, let us consider a dielectric plate placed in a homogeneous waveduide and examine the wave propagation in this waveguide. In Fig. 2.1.1, ε_w and μ_w are the waveguide medium permittivity and magnetic permeability, and ε_d , μ_d are the dielectric permittivity and the magnetic permeability, respectively, and S is thickness of dielectric.

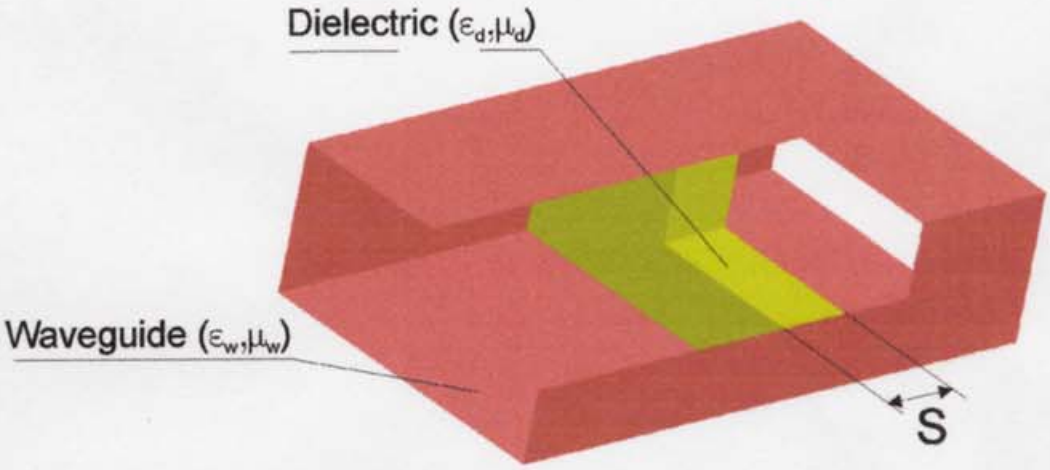

Figure 2.1.1: Dielectric in waveguide.

If an incident waveguide mode impinges on the dielectric plate, a part of wave is reflected, and the rest comes through the plate. If the plate is orthogonal to the waveguide directional line, no other modes are generated. The reflection depends on the thickness of plate and, as the following formula shows, it vanishes when the thickness is a half of the wavelength:

$R = \frac{R_{wd}\left(1-e^{-i2G_d S}\right)}{1-e^{-i2G_d S}R_{wd}^2}$ is reflection from the dielectric plate,

where

$R_{wd} = \frac{Z_d - Z_w}{Z_d - Z_w}$,

$Z_d = \frac{E_{td}}{H_{td}}$ - the wave impedance of mode in dielectric plate

$Z_w = \frac{E_{tw}}{H_{tw}}$ - the wave impedance of mode in waveguide

E_{td}, H_{td}; E_{tw}, H_{tw} - the tangential electric and magnetic field of mode in dielectric and waveguide

G_d, G_w - the longitudinal wave vectors in dielectric and waveguide

$Z_x = Z_{x0}\frac{k_{x0}}{G_x}$ - for TE mode and $Z_x = Z_{x0}\frac{G_x}{k_{x0}}$ - for TM mode (x is d or w)

$Z_{x0} = \sqrt{\frac{\mu_x}{\varepsilon_x}}$ - the wave impedance of plane wave in an infinite medium

$k_{x0}^2 = k_\perp^2 + G_x^2$, where $k_{x0} = \omega\sqrt{\varepsilon_x \mu_x}$ is the wave vector of plane wave

$k_\perp$ - the transverse wave vector, which is determined by the waveguide geometry

For the single mode case, the ways of calculations of a reflected wave, of transmitted wave and even fields are the same as for connection of lines with impedances equal to the wave impedances of modes (see Fig. 2.1.2). Analyses of this simple window can be done by methods of the circuit theory. We skip the algebraic manipulation and present only the final results here. The passband of half-wave window and fields in the dielectric are presented in Figs. 2.1.3 and 2.1.4, respectively. The size of waveguide is 22.86 mm x 10.16 mm. The dielectric permittivity is 9.8. The dielectric thickness is 4.272 mm. The frequency of field calculation is 11.424 GHz. We can see that the waves before and after the dielectric are pure travelling-waves. The wave in dielectric has a big fraction of standing wave. The dielectric serves as a resonator.

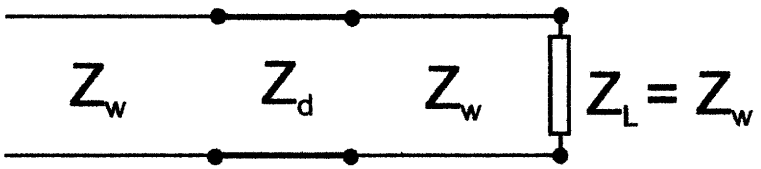

Figure 2.1.2: Equivalent circuit of dielectric in waveguide.

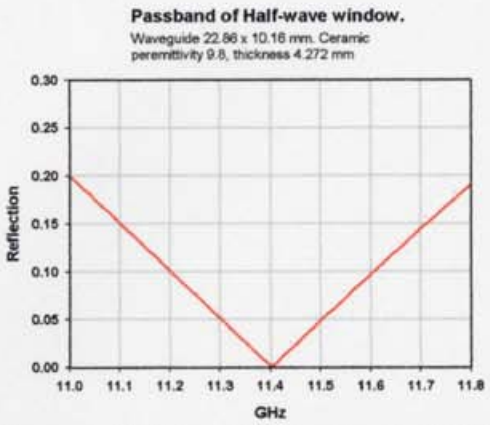

Figure 2.1.3: Passband of half-wave window

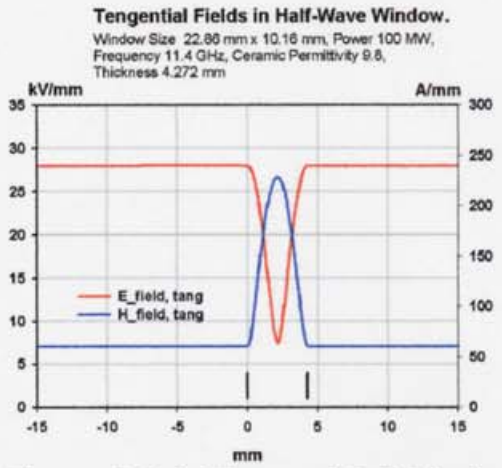

Figure 2.1.4: Tangential fields in half-wave window

At the same time, it is obvious that the waveguide wave carrying a fixed amount of power has the minimum fields when it is a pure travelling-wave. The dielectric in waveguide can be considered as a piece of waveguide. So if we want to decrease the fields on and in the dielectric, we should organize a pure travelling-wave in it. This kind of window is called Travelling Wave Window (TW Window). But how can we form a pure travelling-wave in dielectric? Let us consider an infinite waveguide, a half of which is filled by dielectric. The incident wave coming from the empty waveguide is reflected at the dielectric surface because of different wave impedances (see Fig. 2.1.5). However, by placing a proper matching iris in the empty waveguide, one can eliminate the reflected wave. In this case, we have a pure travelling wave before the matching element and in the waveguide with dielectric. Figure 2.1.6 shows the strength of electric and magnetic fields in this case. The fields in the empty waveguide are normalized to one. We can see that before the matching element and in dielectric the wave is pure travelling-wave. The electric field in dielectric is about a half of the field before the matching element. The theoretical ratio is $\sqrt{Z_d / Z_w}$. We have an electric field surge in the place between the matching element and dielectric. But this is the area of metal in vacuum. And the breakdown limit of metal in vacuum is about one order of magnitude higher than, for example, Al_2O_3 – one of the best dielectrics for windows.

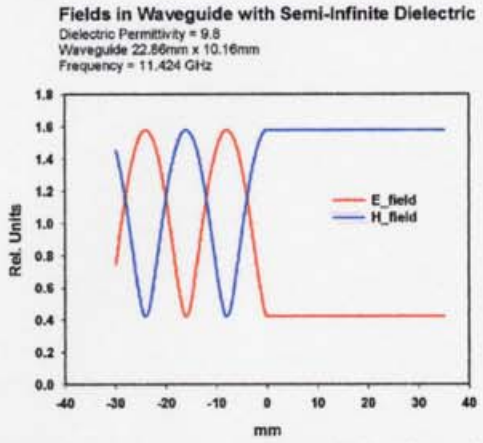

Figure 2.1.5: Tangential electric and magnetic fields in waveguide with semi-infinite dielectric.

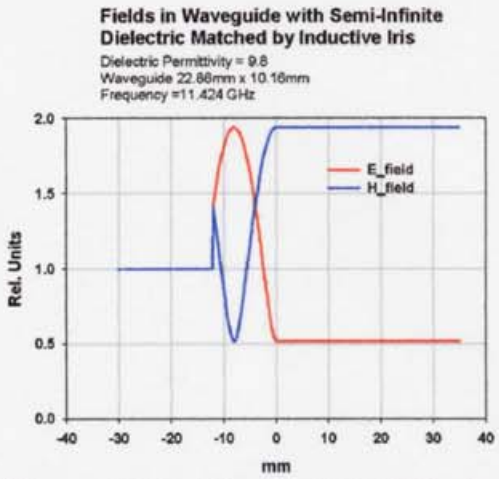

Figure 2.1.6: Tangential fields in waveguide with semi-infinite dielectric and matching element.

To produce a window from the previous geometry, one has to just add a mirror geometry relatively to any plane in dielectric, which is orthogonal to the waveguide propagation direction. Figure 2.1.7 shows the fields in such a window. An equivalent circuit of TW window is presented in Fig. 2.1.8. Taking into account the dependence of parameters on the frequency, we can calculate the window passband. From the above explanation, it is clear that the window matching at the operating frequency does not depend on the dielectric thickness. This is one of advantages of TW window. We can change freely a thickness of dielectric to move reconances from the operating frequency. However, the passband depends on the dielectric thickness. Calculations show that the window has the maximum passband when the dielectric thickness is a quarter of the wavelength. Figure 2.1.9 presents passbands of TW window with a half- and a quarter- wavelength dielectric thickness. For comparison, the passband of half-wave window is presented as well. We can see that the passband of TW window with quarter-wave dielectric is wider than the passband of half-wave window. Another advantage of TW window is a lower density of dielectric resonances (ghost modes) because the thickness of dielectric is one half. The passband of TW window can be made even wider if the window is slightly 'unmatched'. Figure 2.1.10 shows the passband of 'unmatched' TW window.

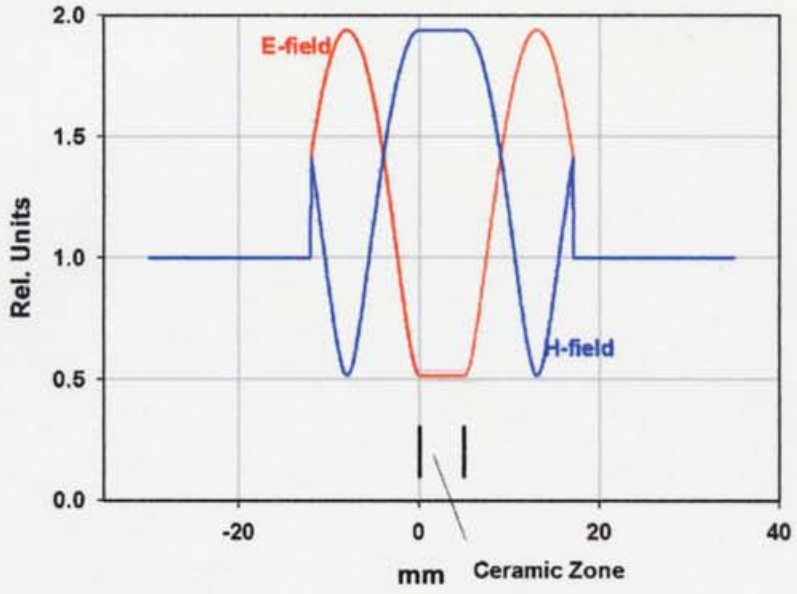

Figure 2.1.7: Tangential electric and magnetic fields in TW window.

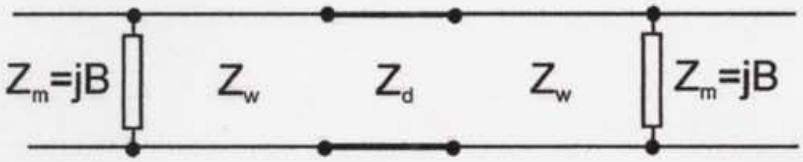

Figure 2.1.8: Equivalent circuit of TW window.

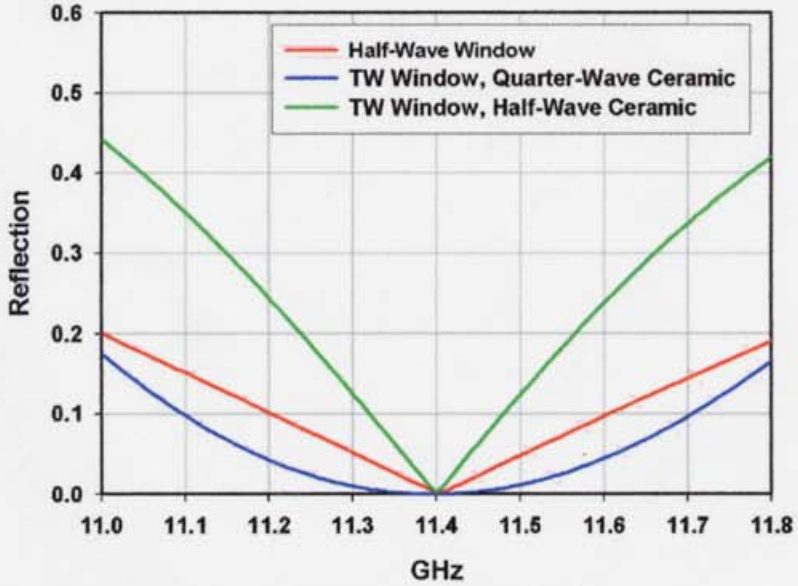

Figure 2.1.9: Passband of half-wave and TW windows.

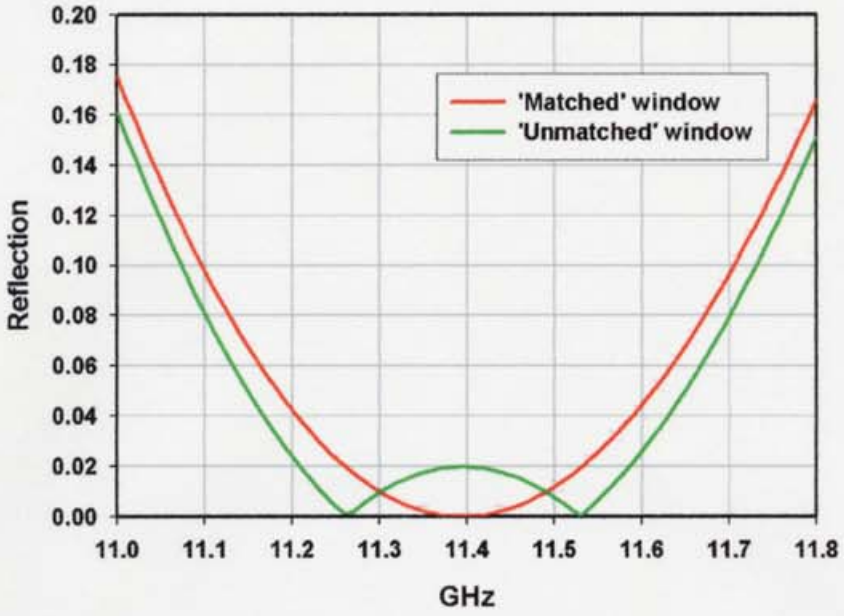

Figure 2.1.10: Mismatching can increase the passband of TW window.

Figure 2.1.11 shows how the maximum electric field on dielectric depends on the diameter of the dielectric for TW windows and half-wave windows. The TE_{11} and TE_{01} modes are chosen as operating modes. The passing power is 100 MW and the dielectric permittivity is 9.8. It is clear that the half-wave window should need the dielectric diameter about twice larger for the same maximum electric field. But the half-wave window has a dielectric twice thicker. Thus the density of resonanses of half-wave window is several times higher than the TW window. Figure 2.1.12 shows the average distances between ghost modes for half-wave window and TW window vs. the maximum electric field on the dielectric. The power is 100 MW. In this figure only the ghost modes are presented; one should also consider volume resonances, which depend on each window geometry. Experiences say that the density of volume resonances is comparable to that of ghost modes. Windows for X-band power sources of a Linier Collider should have a passband about 100 MHz. The electric field limit for Al2O3 ceramic is about 8 kV/mm. This value corresponds to 60 MHz distances between ghost modes for the half-wave window. When the volume resonsnces are included, the distance is even smaller. It means that it is difficult to design a half-wave window with 100 MHz passband for 100 MW power and still free from resonances in the passband. For the TW window, this power limit is about four times higher.

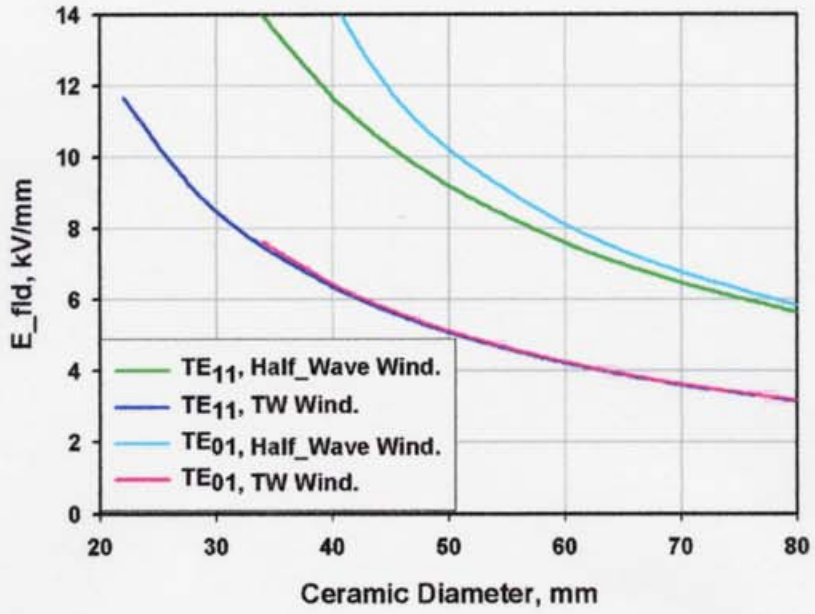

Figure 2.1.11: TE_{01} and TE_{11} half-wave and TW windows. The maximum electric fields on ceramic surface vs the ceramic diameter. Power is 100 MW.

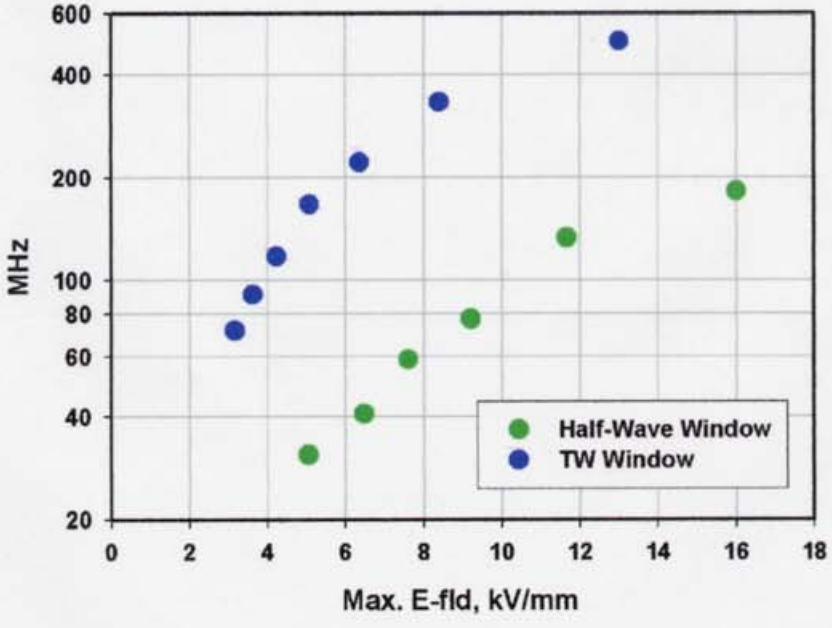

Figure 2.1.12: Average distance between ghost modes of half-wave and TW windows vs the maximum electric field on the ceramic. Power is 100 MW.

2.2 Summary

The new type of RF window with travelling-wave in dielectric was proposed. The window has a low electric field around the dielectric. The electric field of TW window on the dielectric is $\sqrt{Z_d / Z_w}$ times lower than the field of half-wave window. For the ceramic Al_2O_3 with permittivity 9.8, this factor is about 0.5. The window has a wider passband than the half-wave window. The optimal thickness of dielectric is about a quarter of wavelength. It is a half of that for half-wave window. As a result, the TW window has a smaller number of ghost-modes. The lower field causes lower thermal losses.

Chapter 3

S-band travelling-wave window

3.1 Design of S-band TW window

To check the principle of window with travelling-wave in dielectric (TW window), the high power model of S-band window in the operating frequency of 2856 MHz was designed and manufactured [12]. To make the comparison simpler between the new window and a traditional pillbox window, the diameter of ceramic of TW window was chosen to be equal to the diameter of pillbox window, which was tested and used at KEK. The cut-away view of window and the main sizes are presented in Fig. 3.1.1.

The thickness of ceramic was chosen to be 7.59 mm. It is close to a quarter of wavelength to provide a wide passband. At the same time, ceramic resonances are far enough from the operating frequency. The cylindrical part of the window was made slightly tapered to remove volume resonances. All calculated resonances (in ceramic and volume) are shown in Fig. 3.1.2.

The calculated passband of window (-20dB level of reflection) is 100 MHz. It is 3.5% of the operating frequency and is enough for application in accelerator engineering. The maximum electric field on the ceramic is 3.1 kV/mm for the 100 MW transmitted power. Figure 3.1.3 shows the passband of window. Figures 3.1.4 and 3.1.5 show the electric and magnetic field distributions for 100 MW power, respectively. The field distribution on the ceramic fits to the TE_{11} mode. If the electric field limit is considered to be 8 kV/mm, which causes ceramic destruction, the maximum transmittable power is 650 MW. Table 3.1.1 summarizes the design parameters of S-band TW window.

Table 3.1.1: Design parameters of S-band TW window.

Frequency	2856 MHz
Passband (SWR < 1.2)	100 MHz
Diameter of ceramic	84.2 mm
Thickness of ceramic	7.59 mm
Permittivity of ceramic	9.8
Max. E-tang. on the cer. surface	3.1 kV/mm (100 MW)
Max. E-norm. on the cer. surface	0.0 kV/mm (100 MW)
Max. E on the metal	18 kV/mm (100 MW)

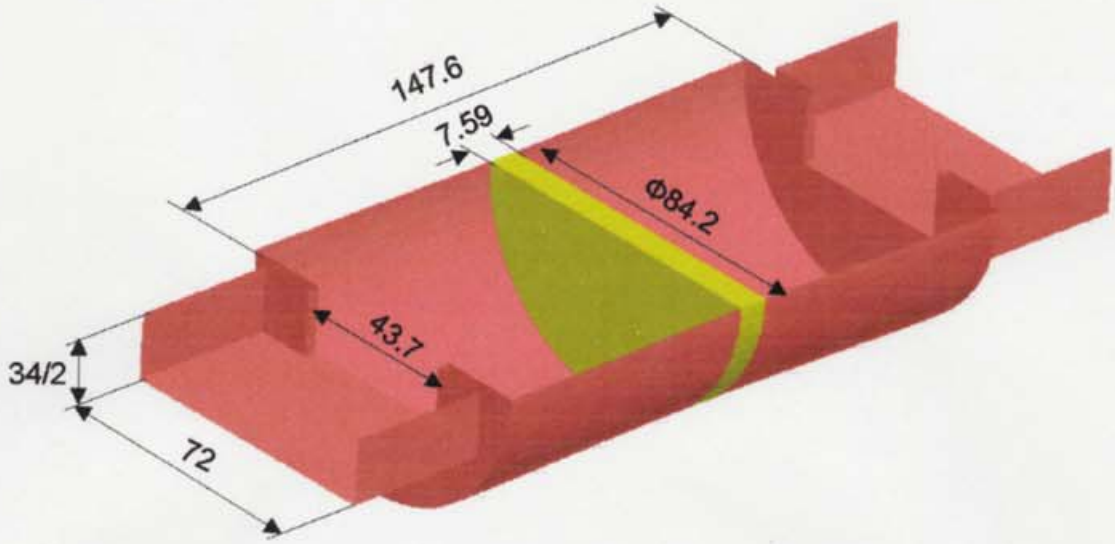

Figure 3.1.1: A cut-away view of S-band travelling-wave window.

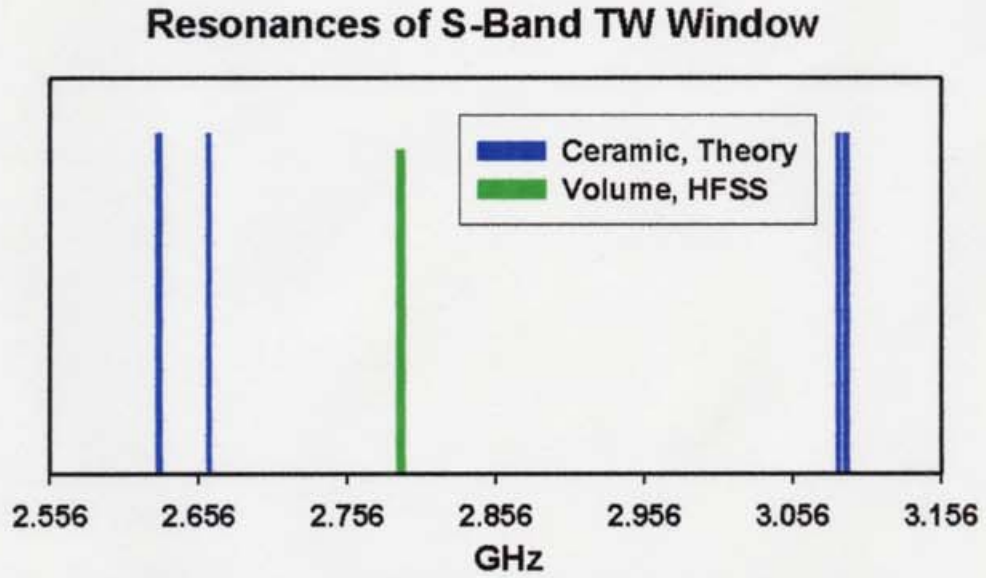

Figure 3.1.2: Ceramic (ghost modes) and volume resonances of S-band travelling-wave window.

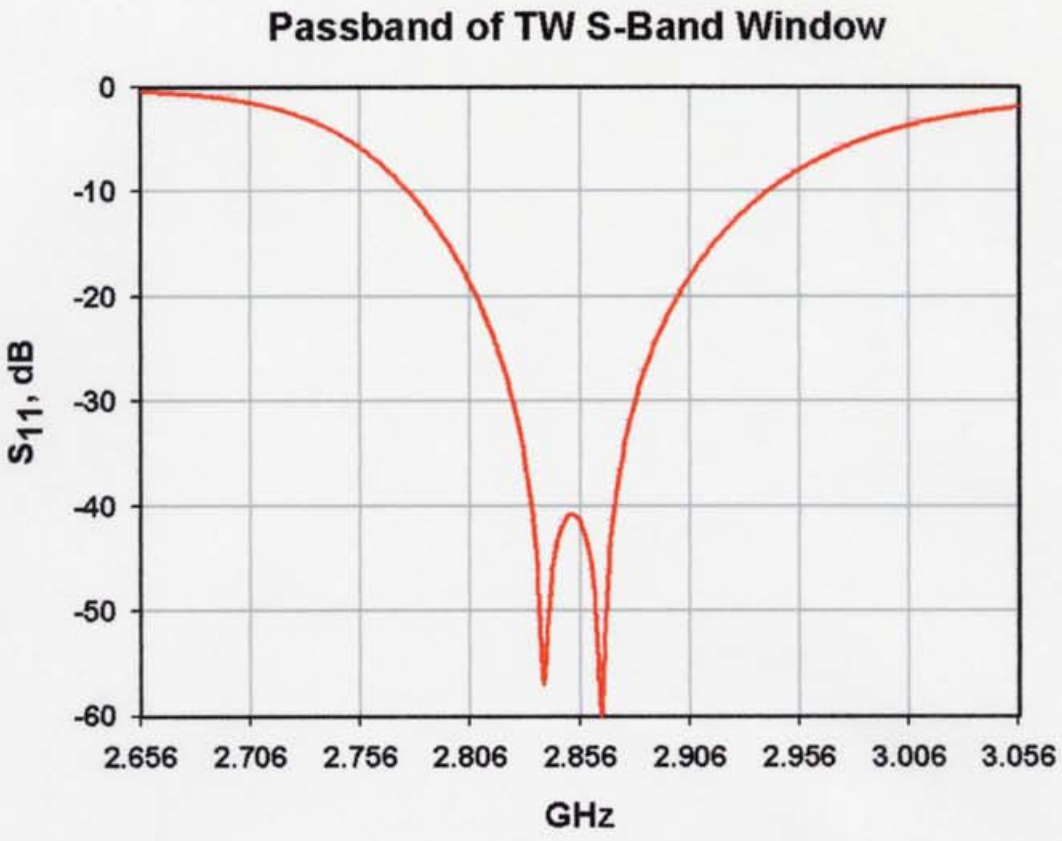

Figure 3.1.3: Passband of S-band travelling-wave window.

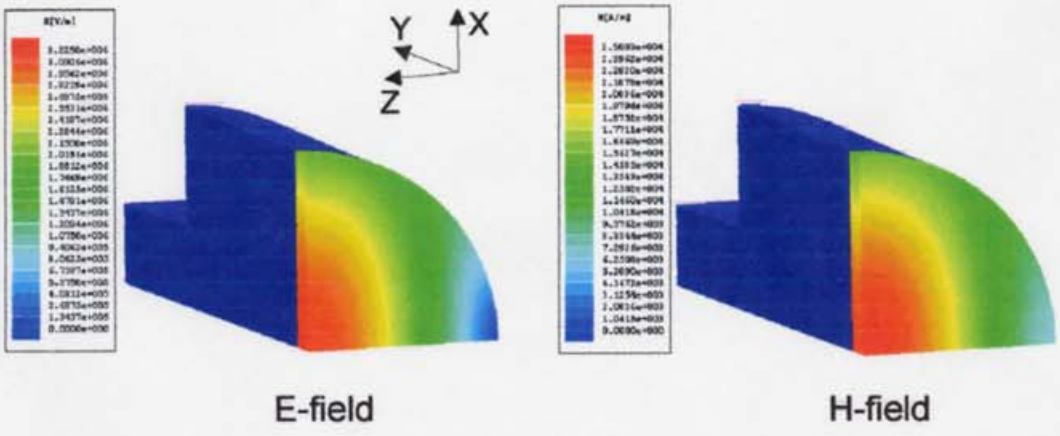

Figure 3.1.4: Electric and magnetic field distributions on the ceramic surface of S-band travelling-wave window at 100 MW power.

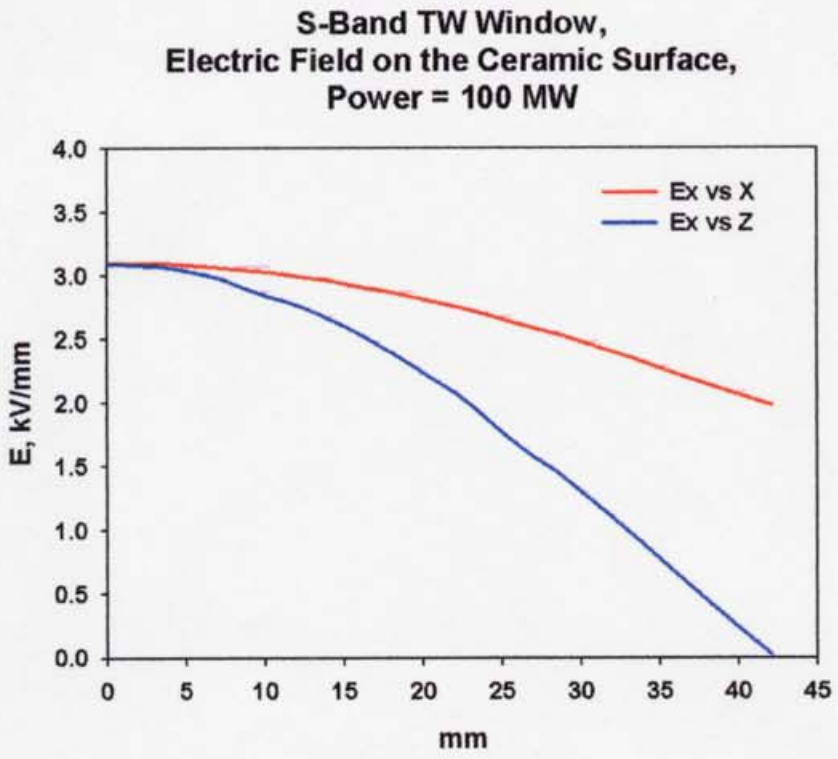

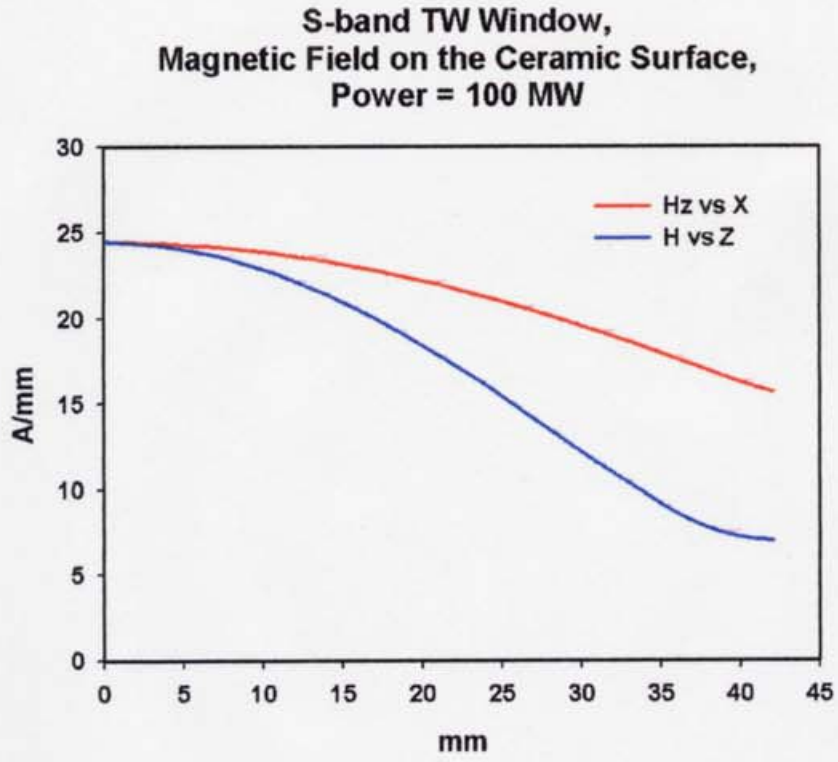

Figure 3.1.5: Electric and magnetic field distributions on the ceramic surface of S-sand travelling-wave window at 100 MW power.

3.2 High power test of S-band TW window

A high power model of this window was manufactured by BINP, Protvino. It is shown in Fig. 3.2.1. Two types of ceramic were used: HA997 made by NTK, Japan and the ceramic made by "Istok", Russia. All ceramics except one were coated by 1.5 nm-thick film of TiN to reduce the secondary electron emission and suppress the multipactor discharge. The high power test was carried out at KEK. The window was installed in the resonant ring fed from a pulsed-klystron (30 MW, 2856 MHz, 2 μs, 50 pps). The configuration of the resonant ring is shown in Fig. 3.2.2. The resonant ring allows to test the window at the maximum power of more than 450 MW. The pressure lower than 10^{-6} Pa was maintained during the operation. The windows were water-cooled and the estimation of thermal losses could be done. Through the view-port, one can observe glowing and breakdown flashes on the ceramic.

The TW window clearly demonstrated very good performances. It was capable of transmitting about twice more power than a pillbox type window without destruction. The TW window with HA997 ceramic was processed up to 470 MW at 2 μs and 50 pps. The plot of processing history is presented in Fig. 3.2.3. Figure 3.2.4 shows the typical pulse shape in the resonant ring. The pulse energy is expressed through the maximum power as $E = 2.16 \frac{J}{MW}$ for this pulse shape (470 MW $\Leftrightarrow$ 1 kJ). As we can see from the processing history, the power was raised up to 400 MW without breakdown. After that, some breakdowns occurred. But the window was operated for longer than 1.5 hours without breakdown at the power of 450 MW at the end of processing. We should note that this level of power is close to the limit of the resonant ring. The intensive x-ray radiation was observed from the phase shifter region. It could be one of the reasons of breakdown.

The quality of a window depends, certainly, on the quality of ceramics. The window with "Istok" ceramics was destroyed at power of 200 MW. The both windows with HA997 ceramic with and without TiN coating were processed to the power of more than 450 MW and were not damaged. However, the intensity of the luminescence of uncoated ceramics was about 10 times more than the luminescence of coated one. The thermal losses were higher for uncoated ceramic. Figure 3.2.5 plots the thermal losses in ceramic per volume unit for different types of windows and for different ceramics. We can see that the losses of TW window are lower than the losses of pillbox window. It can be explained by the lower electric field in the ceramic.

The windows were examined for the vacuum tightness after the high power test. All the windows with HA997 ceramics were vacuum tight. Figure 3.2.6 shows the ceramic surfaces after the test.

There is another interesting advantage of S-band TW window. The ceramic is relatively thick (7.59 mm) and has a large area of brazing. It provides a high mechanical strength. For example, the TW window was exposed to pressure of 10 atm. The window was not destroyed and has kept its vacuum tightness. This experiment indicates that this kind of window can be used in gas-filled systems under high pressure.

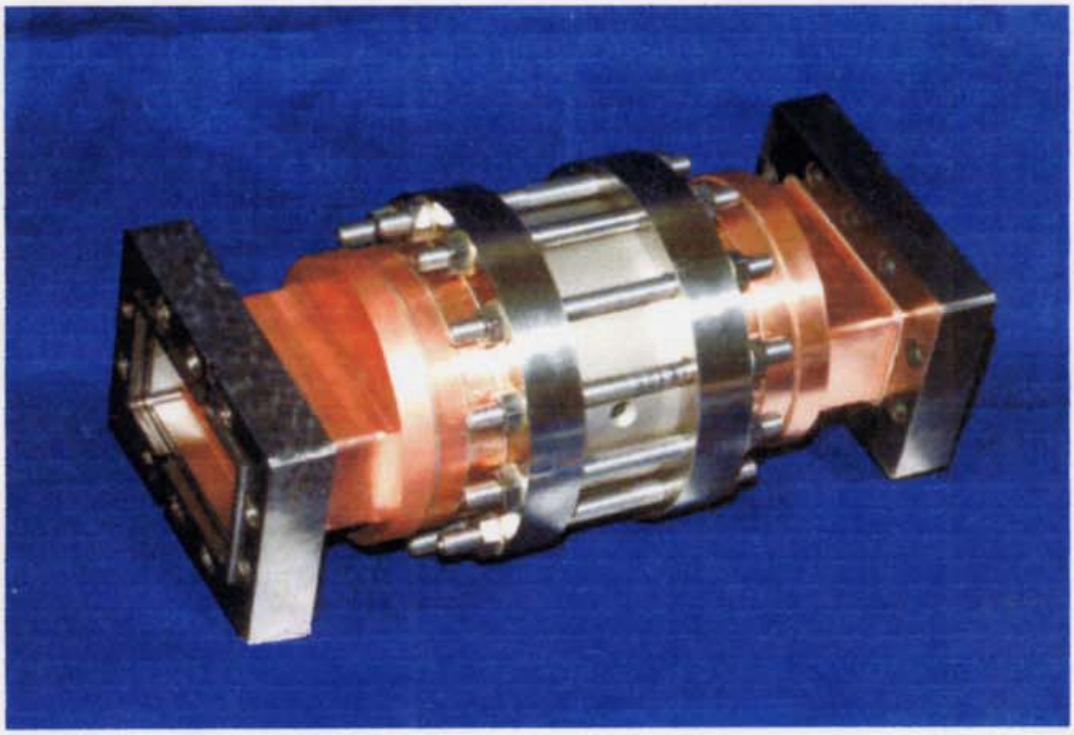

Figure 3.2.1: High power model of S-band travelling-wave window.

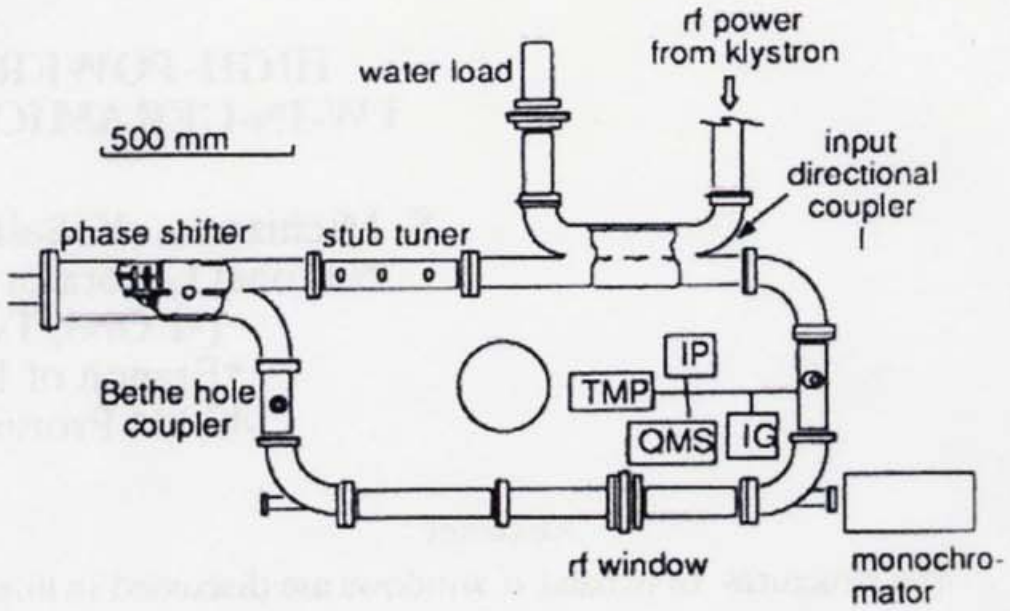

Figure 3.2.2: The resonant ring configuration.

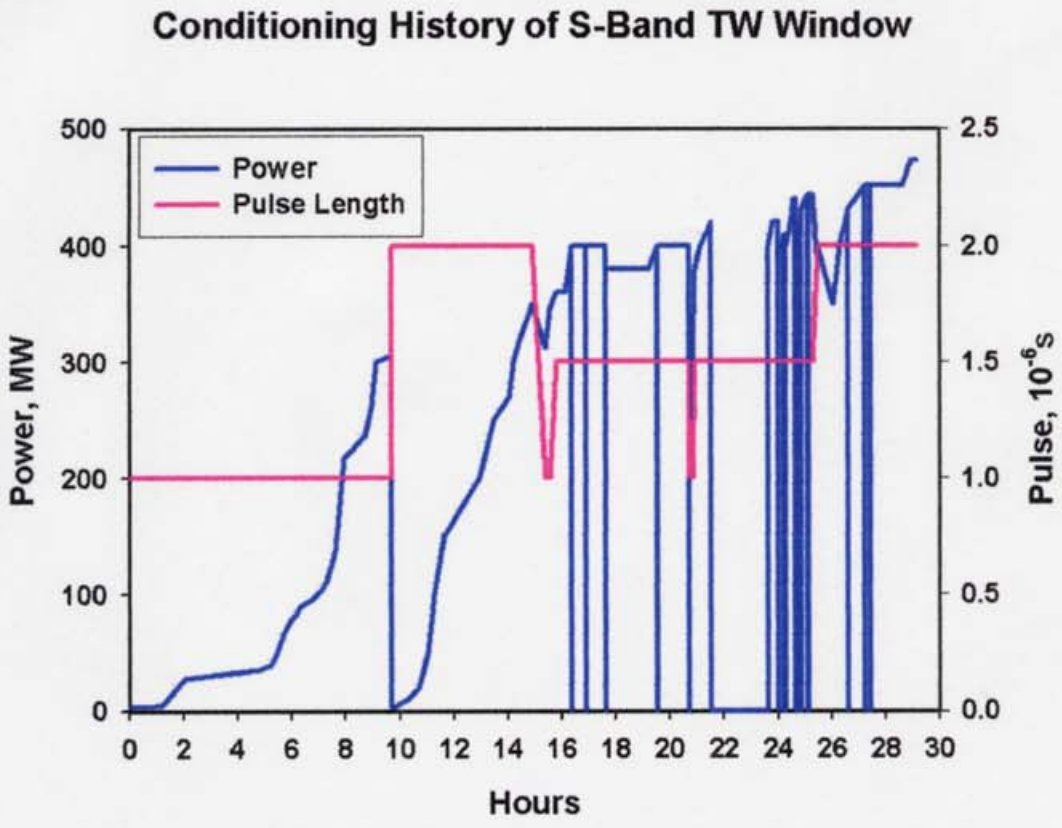

Figure 3.2.3: The processing history of S-band travelling-wave window.

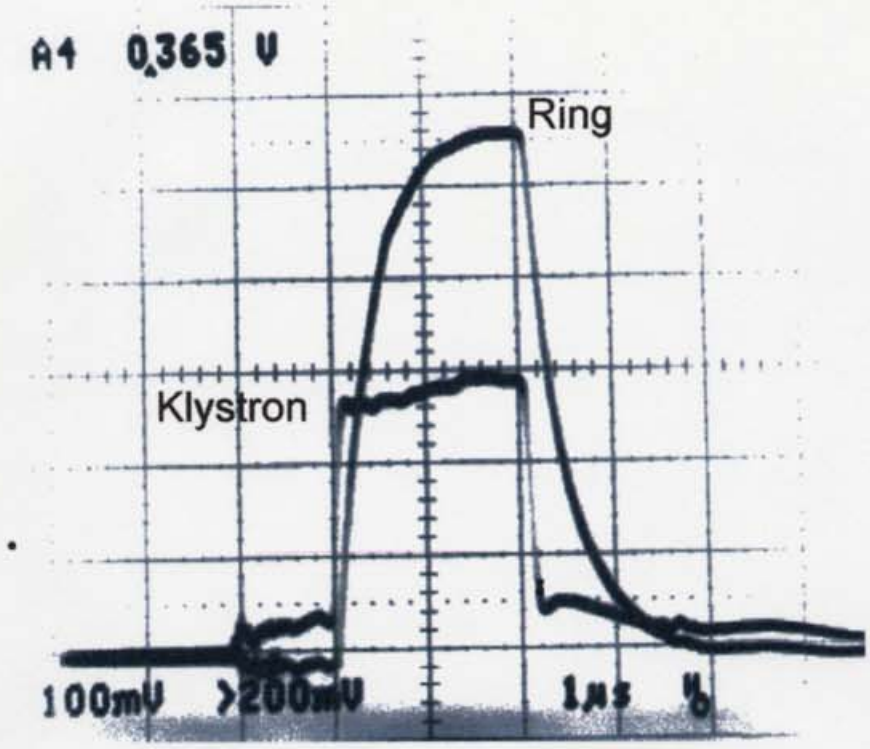

Figure 3.2.4: Typical pulse shape in the resonant ring.

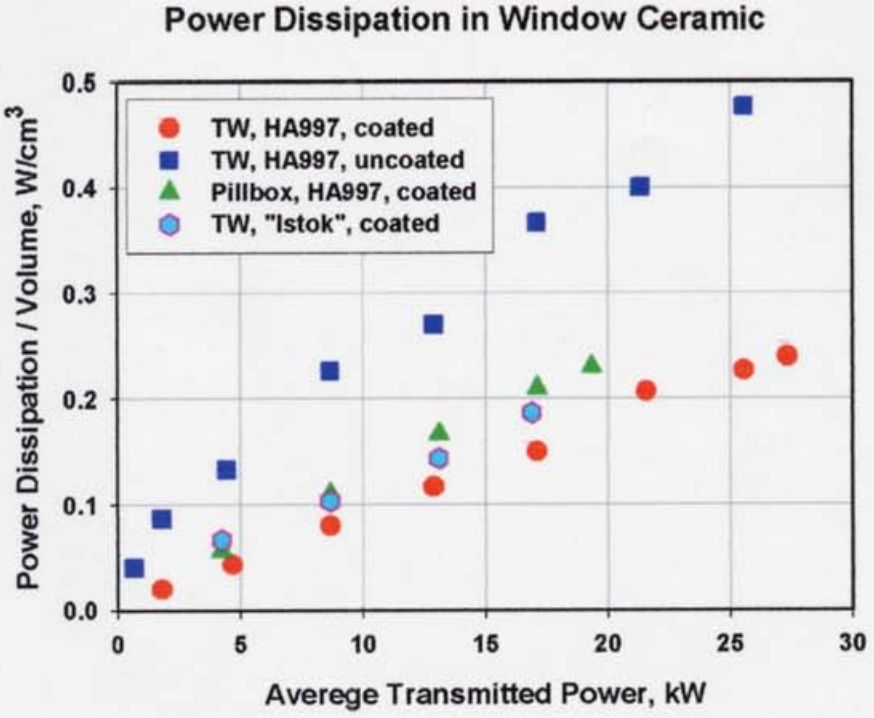

Figure 3.2.5: Power dissipation in the ceramic for different windows.

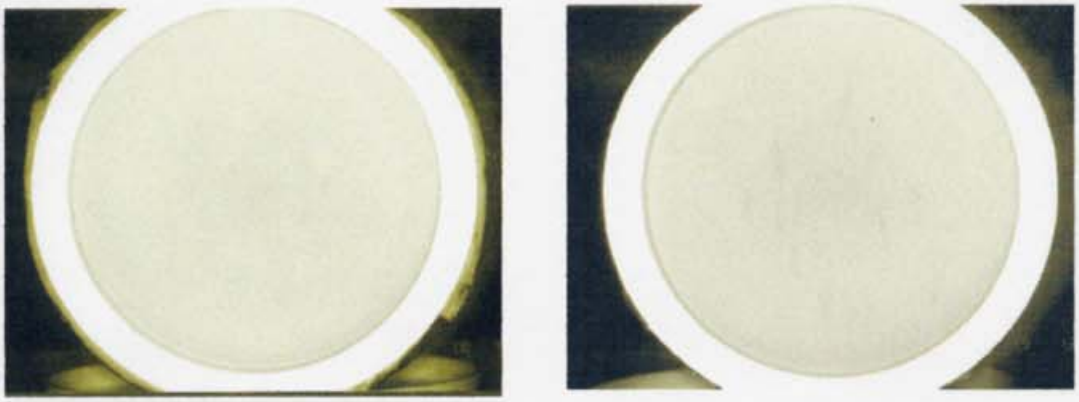

Figure 3.2.6: Ceramic surfaces of S-band travelling-wave window after the high power test.

3.3 Summary

The new type of Travelling-Wave window for S-band was designed, manufactured and tested at high power. The window demonstrates excellent performances. It was capable of transmitting at least twice more power than a typical pillbox window. The TW window was processing up to **470 MW** at **2 μs** pulse length and **50 pps** repetition rate. This is, probably, the best result for S-band windows up to date.

Chapter 4

X-band travelling-wave mixed-mode window

4.1 TE_{11} – TM_{11} mode combination

Experiences tell us that the weakest point of a window is the place of brazing between the ceramic and the metal. The study of broken window shows that this place shows more signs of breakdowns than other parts. A reason can be non-ideal brazing. High electric fields might be present on the sharp edges of metallizing film or solder, which can also cause breakdown. Therefore it is desirable to create a window with low electric field in the brazing area. It is especially important for X-band windows, since the power density and the average strength of field is much higher than S-band windows.

To have the electric field zero at the place of brazing, it is possible to use the window with TE_{01} mode as the operating one. This method was chosen by SLAC [15]. The result of simulation and some characteristics of TW TE_{01} window designed by SLAC are presented in Appendix 4. However, the TE_{01}-windows have a disadvantage too, such windows need TE_{10}-TE_{01} mode converters. The output power from a klystron is transmitted trough rectangular waveguides with single TE_{10} mode. The input of end user (accelerating structure, for example) is also the single mode rectangular waveguide. Thus, it is necessary to convert the TE_{10} mode of rectangular waveguide to the TE_{01} mode of circular waveguide and to convert it back later. The need of mode converters makes windows more complicated and expensive. In addition, the mode converters increase a window volume that results in narrowing passband and increases the number of parasitic resonances.

However, it is possible to get a low level of electric field on periphery of ceramic (place of brazing) by combining different modes with an identical number of angular variations [14]. It is clear from Fig. 4.1.1, which illustrates the distributions of electrical field as a function of the radius for TE_{11} and TM_{11} modes. We can see that the tangential electric fields of these modes have different signs at periphery, and the normal component of TM_{11} mode is vanishes because of the boundary conditions. The TE_{11} mode has no normal component. It means the summation of TE_{11} and TM_{11} mode with appointed coefficients can have zero field on periphery. Figures 4.1.2 – 4.1.4 show fields of TE_{11}, TM_{11} modes and there summation, respectively. We can see that the magnetic field is also low at the periphery. It means the RF current is small at this place. Thus, the

requirements for the quality of brazing would be not too tough while the window should be reliable. As the figure shows, the electric field strength is similar to the axially symmetric distribution. Thus, the ceramic heating must be more uniform and it causes a lower mechanical stress. Playing with the mode coefficients in the summation, we can get different combinations between the maximum electric field and the field on the periphery. Figure 4.1.5 shows the dependences of the maximum electric field on the ceramic surface vs the field at the periphery for different ceramic diameters. The permittiviy of the ceramic was chosen to be 9.8, and the transmitted power is 100 MW.

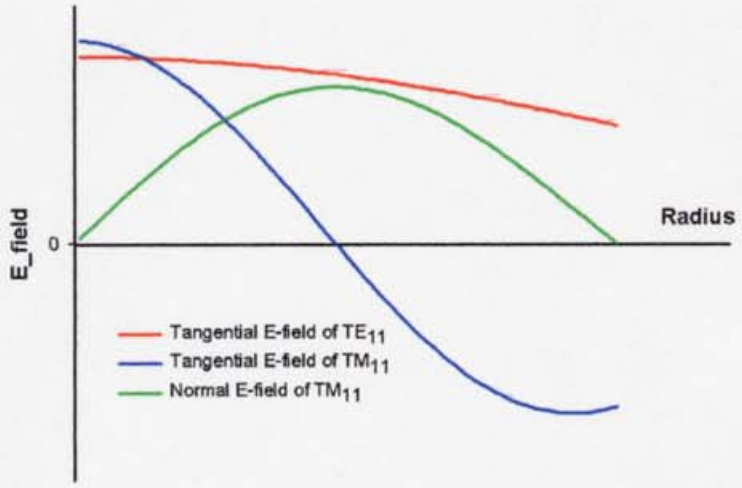

Figure 4.1.1: Electric fields of TE_{11} and TM_{11} modes in the circular waveguide

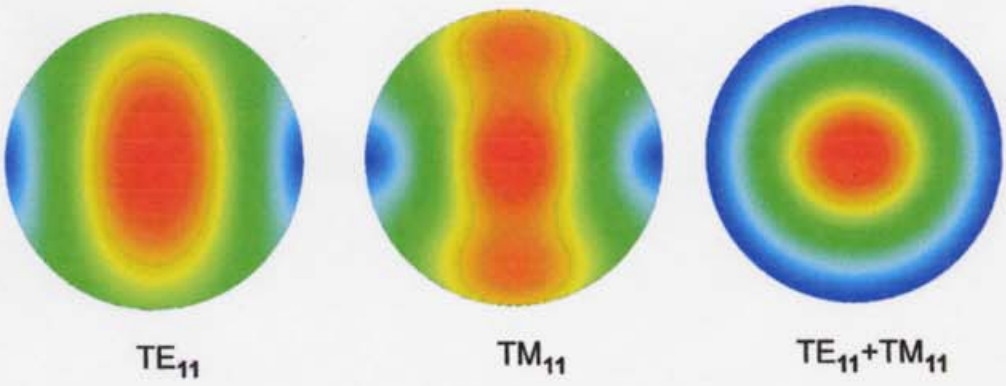

Figure 4.1.2: Electric fields of TE_{11} and TM_{11} modes and their summation in the circular waveguide

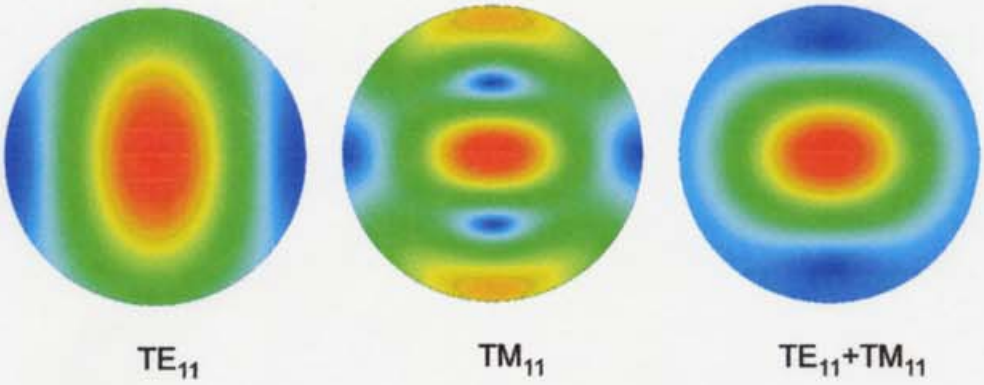

Figure 4.1.3: Magnetic fields of TE_{11} and TM_{11} modes and their summation in the circular waveguide.

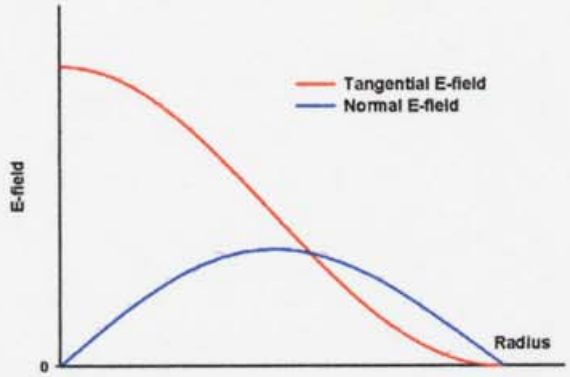

Figure 4.1.4: Electric fields of summation of TE_{11} and TM_{11} modes in the circular waveguide.

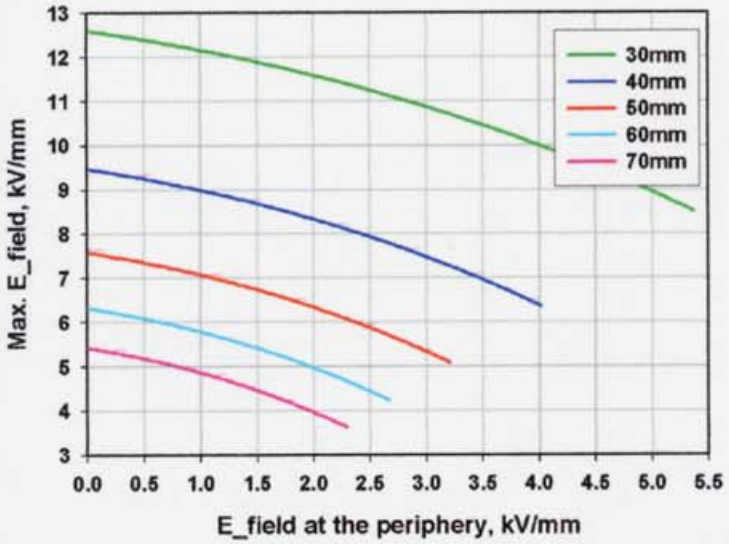

Figure 4.1.5: The maximum of electric field vs the electric field on the periphery for TE_{11} and TM_{11} mode combination in the circular waveguide. The medium permittivity is 9.8. The transmitted power is 100 MW.

4.2 Design of X-band travelling-wave mixed mode window

How can we get the combination of TE_{11} and TM_{11} modes properly? It is easy. The simple smooth transition from rectangular waveguide to circular one provides the TE_{11} mode. The step in the circular waveguide generates the TM_{11} mode. Therefore we need no complicated mode converter. If the radius of circular waveguide after the step exceeds $0.85\lambda_0$, the third TE_{12} mode is generated as well. But TE_{12} has the same features as TM_{11} – the electric field in the periphery has opposite sign compare to the TE_{11} mode. The fraction of TE_{12} mode is noticeably smaller than the fraction of the TM_{11} mode.

It is easy to generate modes, but a more difficult task is to provide travalling-wave conditions in the ceramic for all of them simultaneously. We cannot use the single mode approach placing an appropriate matching iris. All modes have different wave impedances, so that they have different reflections from the ceramic. They have different longitudinal wave vectors and different reflections from the iris. It is hopeless to try to find a common matching iris for all two or even three modes. But we finally managed to find the window shape, which provides the desired mode combination and the travelling wave conditions. At the days of this work, the speed of computer was not fast enough to simulate many shapes of the whole window. The window was divided into parts and the S-matrix of each part was calculated. Combining the S-matrix and changing some parameters, the optimal geometry was found. By knowing coefficients of the S-matrix, the maximum field on the ceramic surface, fields at the ceramic periphery, the stored energy in the window were estimated and minimized. After that, the entire geometry was checked by HFSS. But now the computer progress is fast. Present-day computers are powerful enough and a simulation of the whole geometry takes about 10 min. It makes possible to optimize the window shape as whole by changing more parameters. The new geometry, simpler for fabrication, is presented in Appendix 5.

To our surprise, the window geometry has appeared as very simple, compact and manufacturable. The window has a wide passband. Figure 4.2.1 shows the window geometry. The diameter of ceramic is 53 mm and its thickness is 2 mm. The sizes of ceramics were chosen to remove the ceramic resonanses from the operating frequency as far as possible. Figure 4.2.2 shows the resonances of the window. The window passband is presented in Fig. 4.2.3. The electric and magnetic field distributions are shown in Figs. 4.2.4 – 4.2.7. The main window properties are summarized

in Table 4.2.1. Note that the maximum electric field on the ceramic is 7.8 kV/ mm for 100 MW power. Fields on the metal is 52 kV/mm. It gives a hope that the window will be capable of transmitting 100 MW without distraction. The window was developed for the X-band 75 MW klystron with two output waveguides; the output power is 37.5 MW per window.

Table 4.2.1: Parameters of X-band travelling-wave mixed-mode window.

Operating frequency	11424MHz
Ceramic diameter	53 mm
Ceramic thickness	2 mm
Ceramic permittivty	9.8
Passband (SWR < -1.2)	440 MHz
Max. E-field on the ceramic (100 MW)	7.8 kV/mm
Max. E-field on the periphery (100 MW)	0.44 kV/mm
Max. E-field on the metal (100 MW)	52 kV/mm

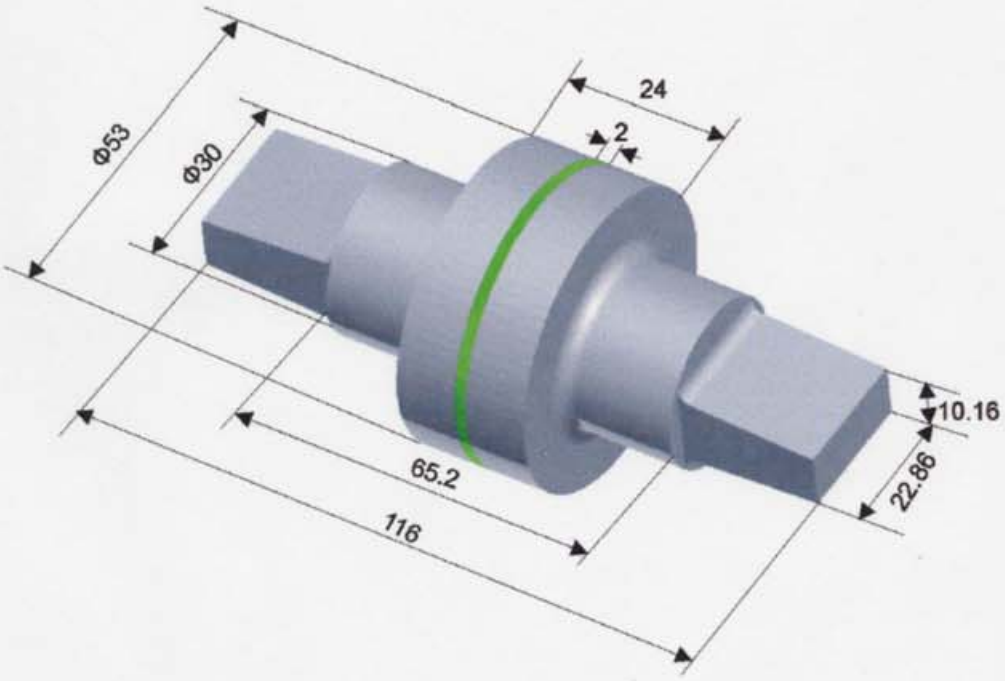

Figure 4.2.1: Geometry of X-band travelling wave mixed-mode window.

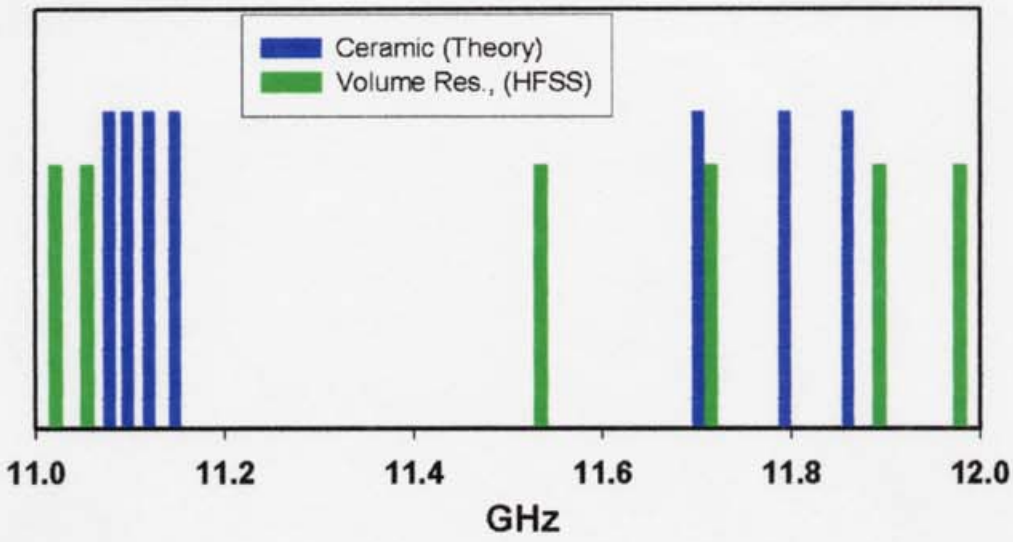

Figure 4.2.2: Resonances of X-band travelling-wave mixed-mode window.

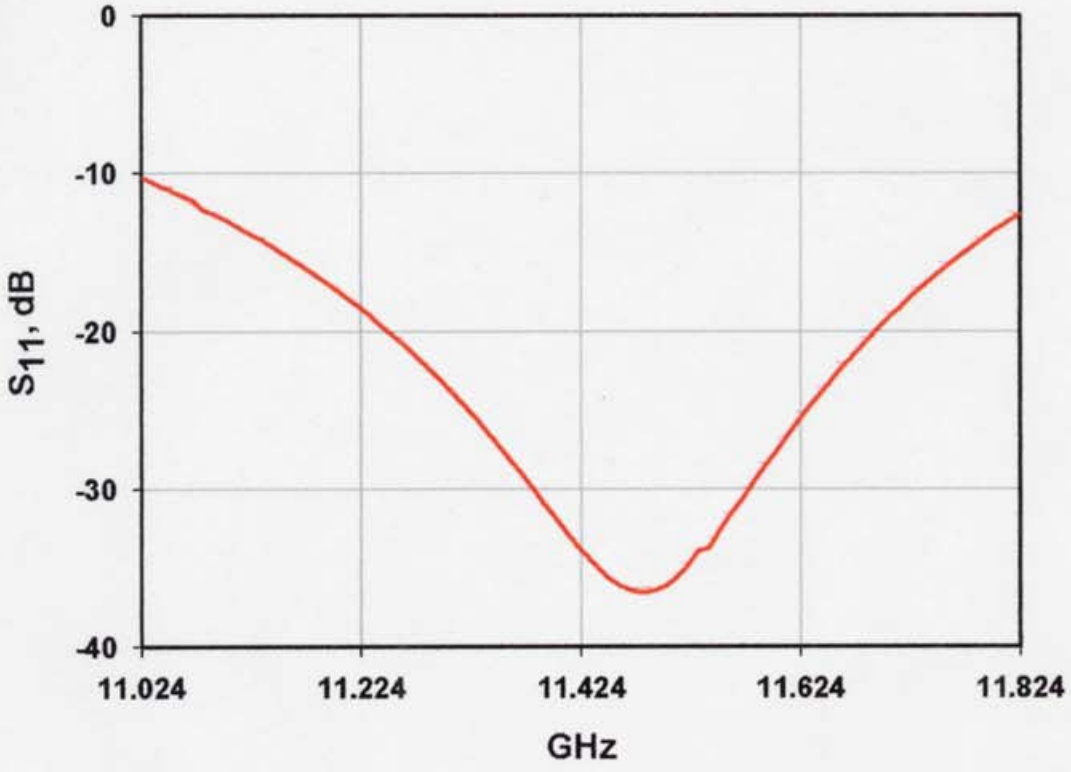

Figure 4.2.3: Passband of X-band travelling-wave mixed-mode window.

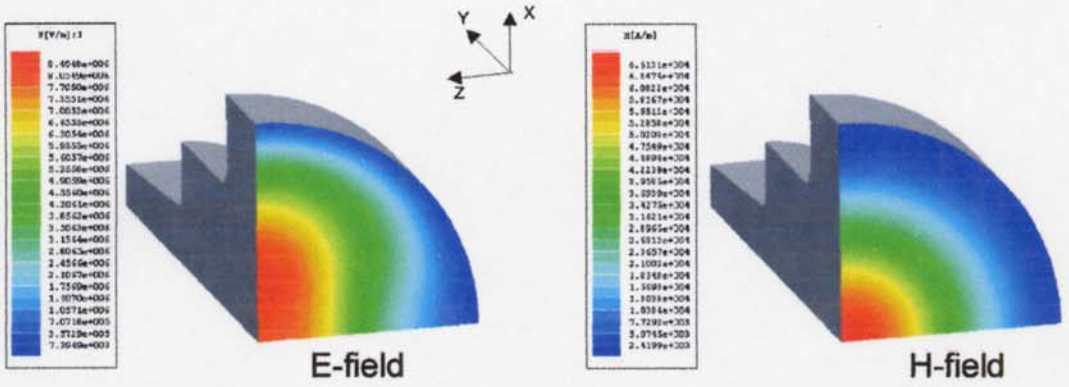

Figure 4.2.4 Electric and magnetic fields distributions on the ceramic of X-band travelling-wave mixed-mode window at power of 100 MW.

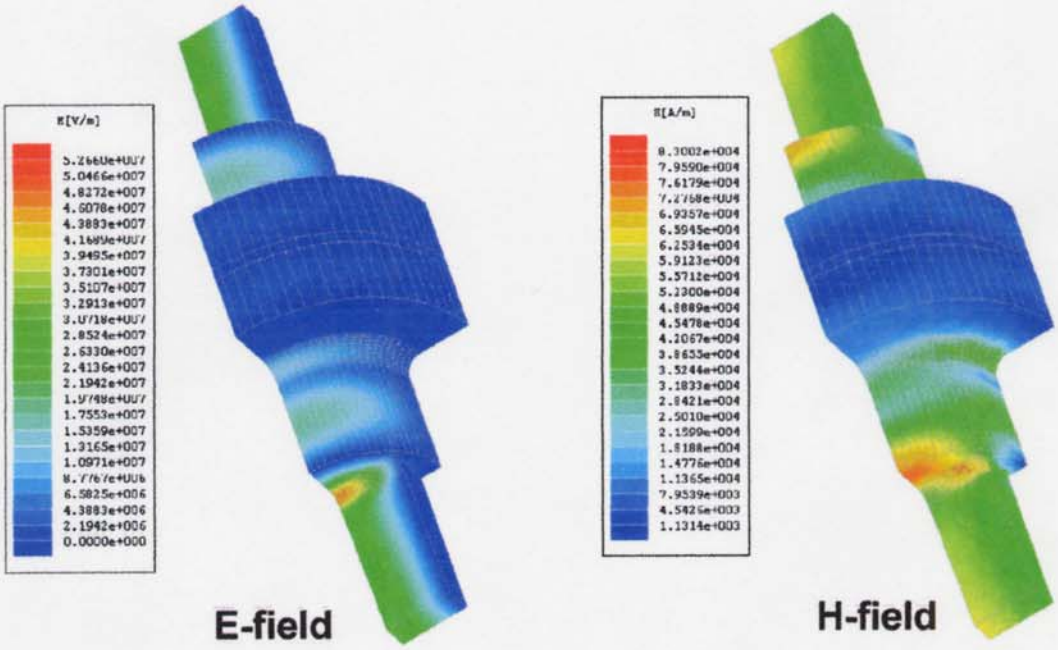

Figure 4.2.5: Electric and magnetic fields distribution on the metal of X-band travelling-wave mixed-mode window at power of 100 MW.

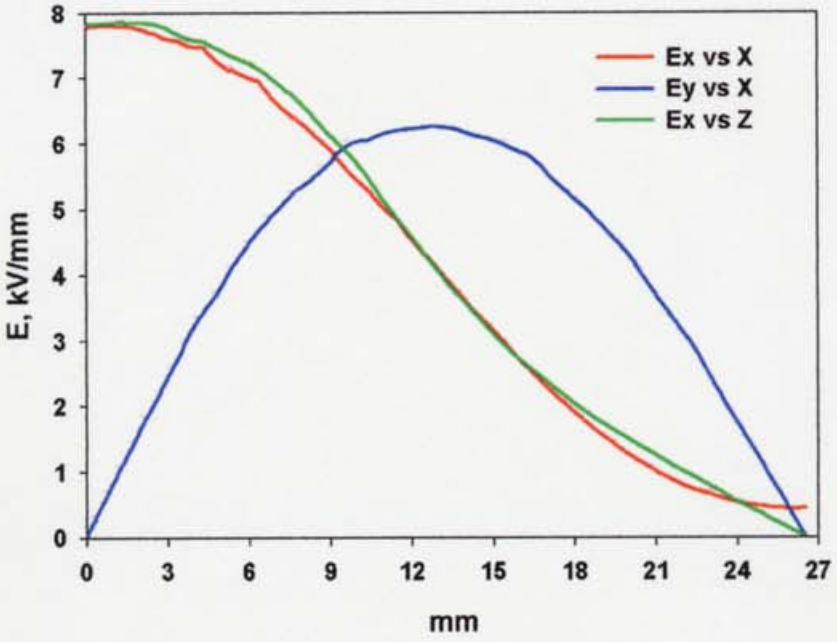

Figure 4.2.6: Electric field on the ceramic of X-band travelling-wave mixed-mode window at power of 100 MW.

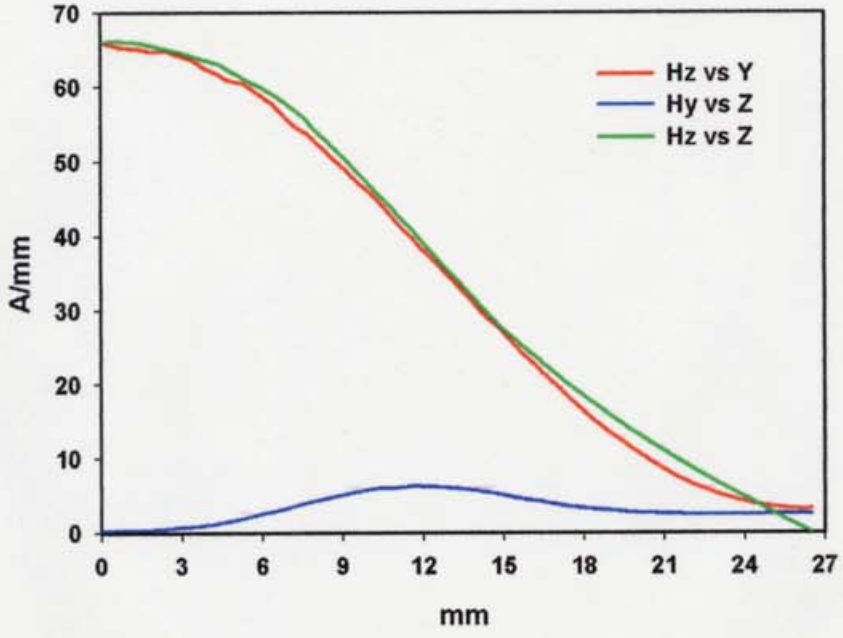

Figure 4.2.7: Magnetic field on the ceramic of X-band travelling-wave mixed-mode window at power of 100 MW.

4.3 High power test of X-band travelling wave mixed-mode window

A high power model was made in KEK, see Fig. 4.3.1. The cold measurements have shown a good agreement with calculation. The window has the passband of 260 MHz at SWR level of 1.1 and 440 MHz at SWR level of 1.2. At the first stage, the high power experiment was carried out at KEK. The window was installed into the resonant ring. The window was conditioned up to 81 MW at 300 ns and 66 MW at 700 ns [16]. The processing history is shown in Fig. 4.3.2. Figure 4.3.3 shows the KEK X-band resonant ring. The experiment was terminated due to time constraints and the window was sent to SLAC to continue the experiment. Then in SLAC, the window was tested by connecting it directly to klystrons without resonant ring. The power of the two klystrons was combined and transmitted to the window. The maximum power achievable in this installation was 110 MW at 1.5 μs pulse length [17].

Figure 4.3.4 shows the experimental setup in SLAC. We should note that the experiment with direct connection to klystron is tougher for windows. In the case of resonant ring, the breakdown absorbs only the energy stored in the resonant ring, which is relatively small. In the case of direct connection, all energy coming from klystron can be taken by breakdown. At the same time the level of higher harmonics is higher in the case of direct connection, which can be dangerous for windows. Nevertheless, the window has demonstrated very good performances. After conditioning, the powers of 100 MW at 0.5 μs and 85 MW at 1.5 μs were achieved [17]. After testing, the window kept its vacuum tightness. The processing history is plotted in Fig. 4.3.5. Now this type of windows is installed in the 75 MW Toshiba E3761 and demonstrates good reliability, see Figs. 4.3.6 and 4.3.7.

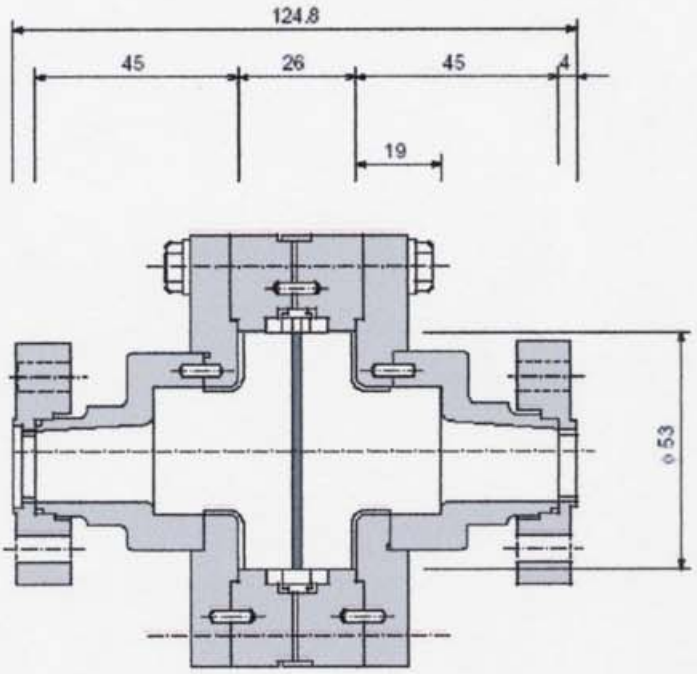

Figure 4.3.1: Drawing of high power model of X-band travelling-wave mixed-mode window.

Figure 4.3.2: X-band resonant ring at KEK.

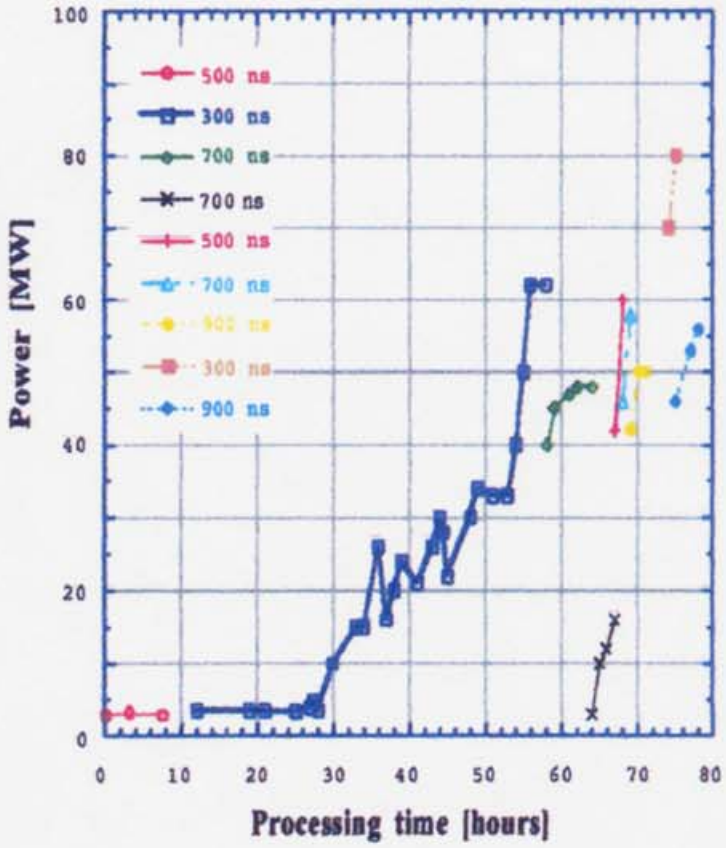

Figure 4.3.3: Processing history of X-band travelling-wave window in KEK resonant ring.

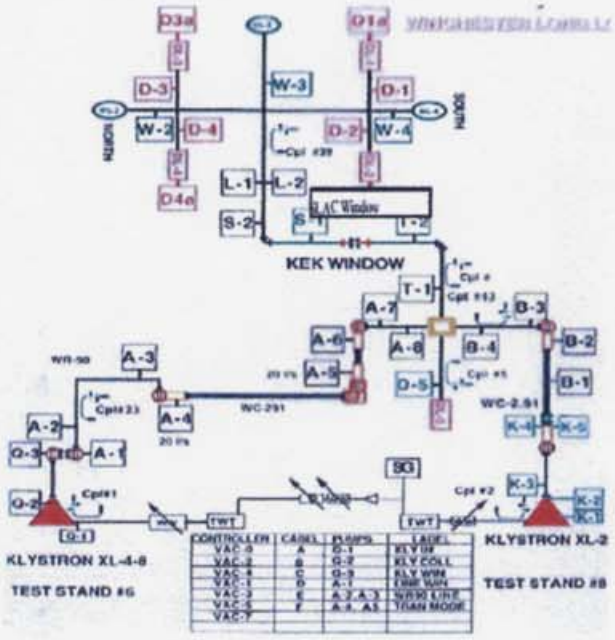

Figure 4.3.4: Setup for high-power window test at SLAC.

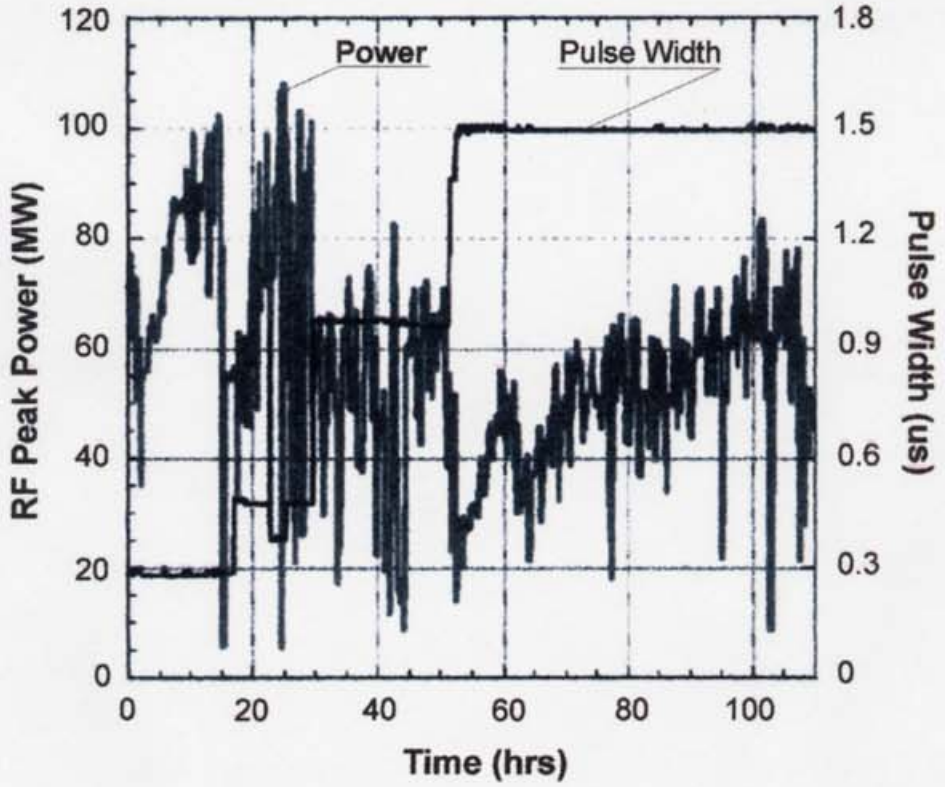

Figure 4.3.5: Processing history of X-band travelling-wave window during test at SLAC.

Figure 4.3.6: X-band travelling-wave window in the 75MW E3761 Toshiba klystron.

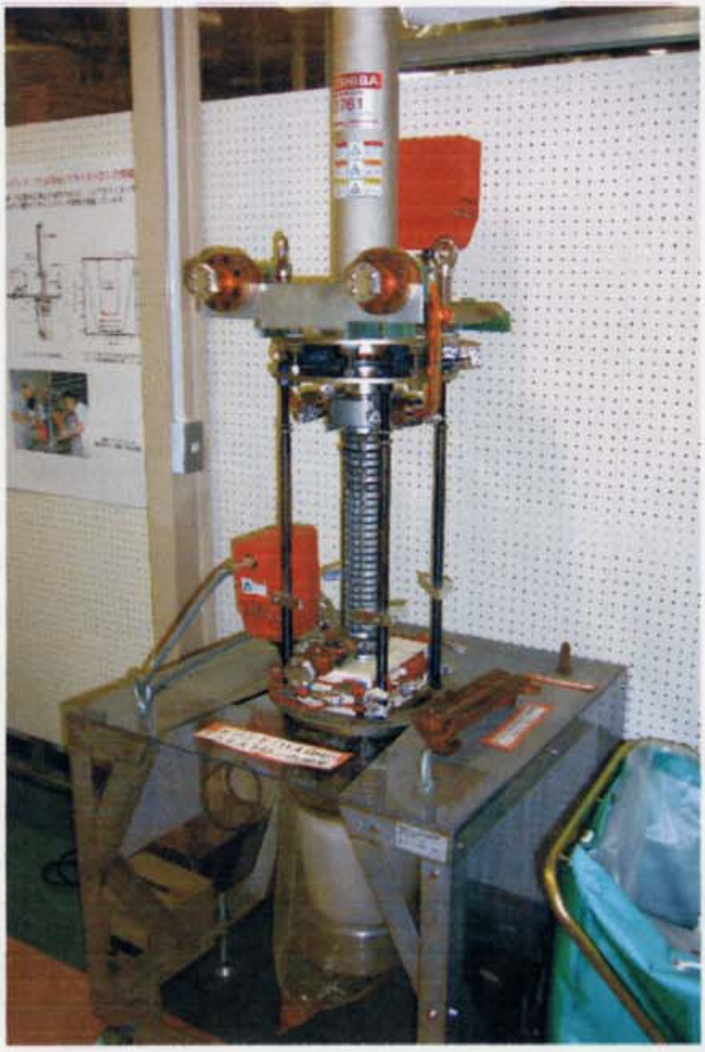

Figure 4.3.7: 75MW E3761 Toshiba klystron with the X-band travelling-wave window.

4.4 Summary

The new type of window with use of the mixed modes was proposed. The window has low electric and magnetic fields in the ceramic-metal brazing area. The travelling-wave conditions for the ceramic provide general field reduction on the ceramic. The window has the very simple, compact and manufactorable geometry. It is also wideband. The high power model of window for X-band was designed and manufactured. The high power experiments showed that the window is capable of transmitting the power of 100 MW at 0.5 μs pulse length and 85 MW at 1.5 μs without distraction. Now this type of window has been successfully used in the 75 MW Toshiba E3761 klystrons.

Chapter 5

X-Band TE_{01}-TE_{02} travelling-wave window

5.1 Design of TE_{01}-TE_{02} travelling-wave window

As it was said in Chapter 1, for complete reliability, a window should be able to operate at power four times higher than required as an RF source. For the 75 MW X–band klystron with two outputs, the window should be capable of transmitting 150 MW power without distraction. In other words, the maximum electric field should not exceed 8 kV/mm for 150 MW (6.5 kV/mm for 100 MW) or even less taking into accounts a further progress of RF sources. It means that we should increase the size of ceramic more if we want to keep lower electric fields in the periphery. From this point of view, a window with TE_{01} and TE_{02} modes looks attractive [18]. In the case of axial symmetry, the TE_{01} mode generates only TE_{02} mode and vice versa if the diameter of system is smaller than $3.24\lambda_0$ (the critical size of TE_{03} mode). In our case, it is 85 mm for 11.424 GHz. So, within this size, the window is double–moded, which simplifies analysis and design. At the same time, the window has zero electric field at the periphery. Certainly, this kind of window demands TE_{10}-TE_{01} mode converters. However we have managed to design a simple and effective mode converter, which can be used for this purpose [19].

It turned out that the geometry of TE_{01}-TE_{02} travelling-wave window is very simple and compact. The window is also extremely broadband. The geometry is presented in Fig. 5.1.1. The size of ceramic was chosen to satisfy the following requirements: the size has to be noticeably less than 85 mm (the TE_{03} mode should decay enough); the thickness has to be close to the quarter of wavelength to produce a wide passband; the combination of diameter and thickness has to provide no ceramic resonance near the operating frequency. Figurer 5.1.2 shows the position of window resonances. Figures 5.1.3 – 5.1.5 demonstrate the principles of choice of ceramic size and show the sensitivities of resonance frequencies to various parameters. Figure 5.1.6 shows the window passband. We can see that this heavily oversized window has the passband of about of 600 MHz at SWR level of 1.2. The electric and magnetic field distributions on the ceramic surface for 100 MW power are shown in Figs 5.1.7 and 5.1.8. The maximum electric field on the ceramic for 100 MW power is 3.77 kV/mm. The low electric field on the ceramic, the absence of electric field in the ceramic-metal brazing area and the absence of electric field on the metal

imply that the window will be able to operate at several hundreds of MW. The main parameters of window are summarized in Table 5.1.1

Table 5.1.1: Parameters of TE_{01}-TE_{02} travelling-wave window.

Operating frequency	11424 MHz
Passband (SWR < 1.2)	600 MHz
Ceramic diameter	77.1 mm
Ceramic thickness	2.12 mm
Ceramic permittivity	9.8
Max. E-field on the ceramic (100 MW)	3.77 kV/mm
Max. E-field on the periphery	0
Max. E-field on the metal	0

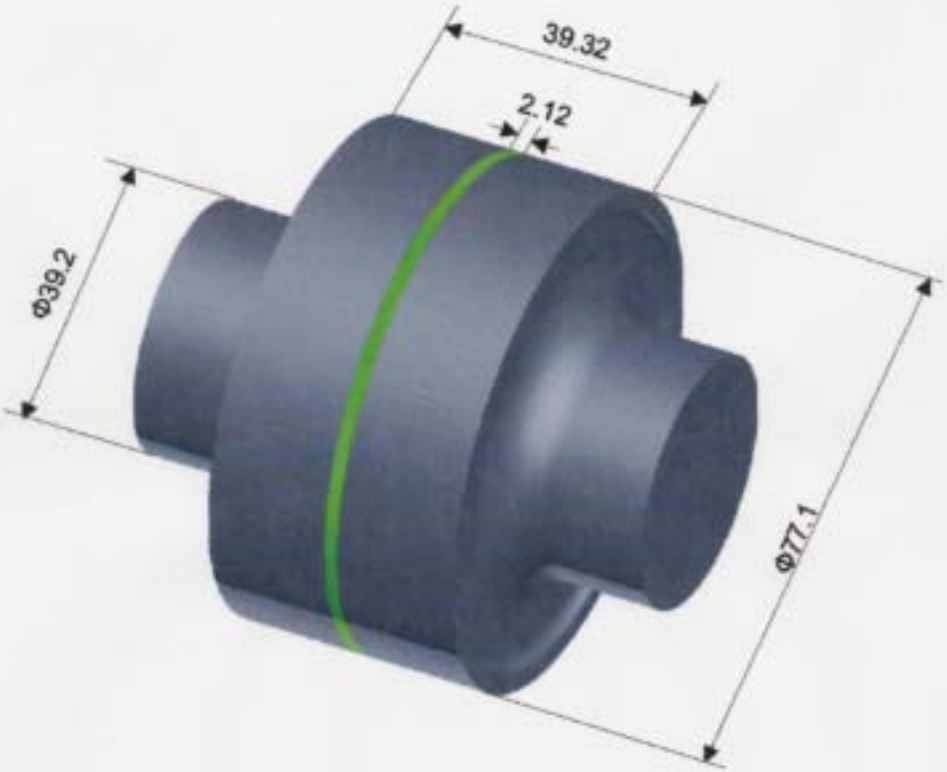

Figure 5.1.1: Geometry of X-band TE_{01}-TE_{02} travelling-wave window.

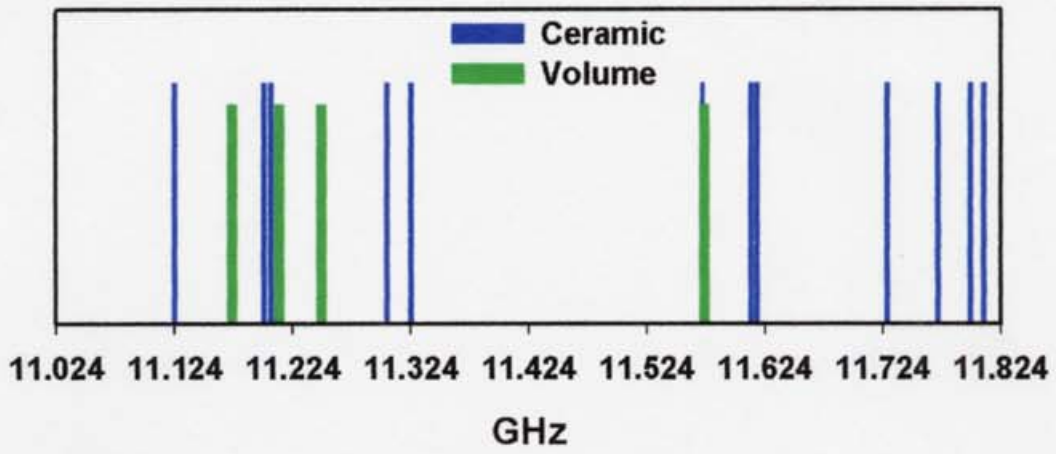

Figure 5.1.2: Resonances of X-band TE_{01}-TE_{02} travelling-wave window.

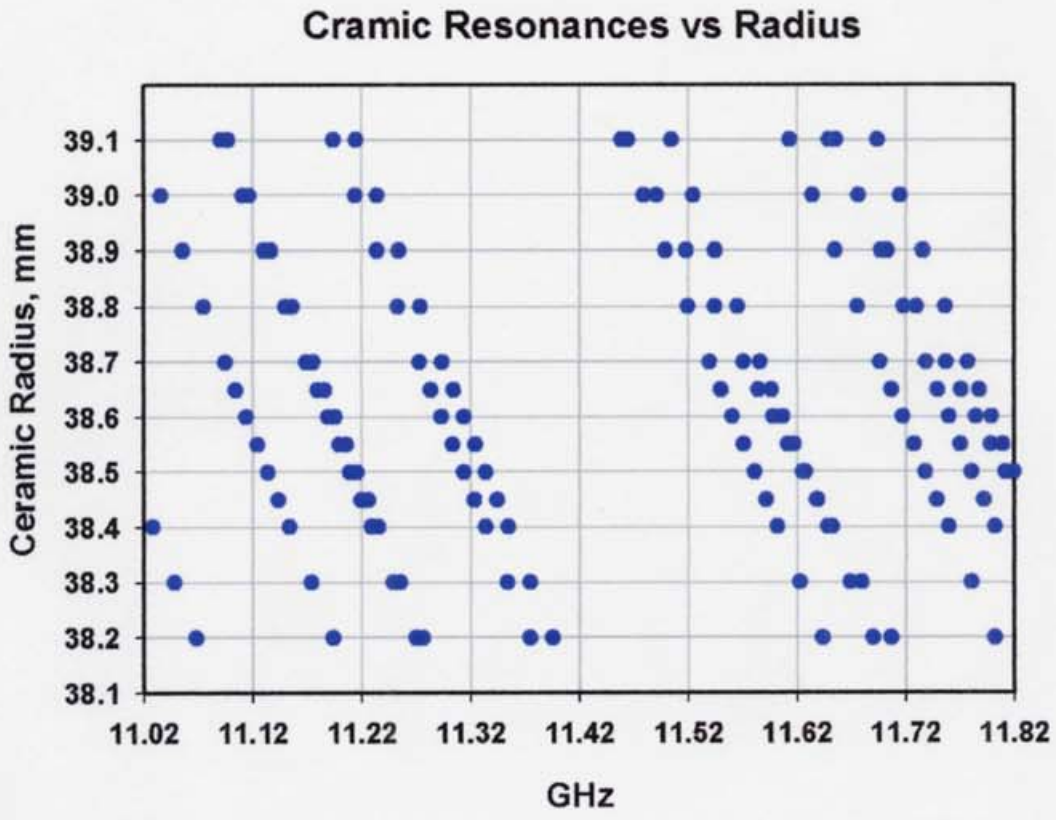

Figure 5.1.3: Dependence of the frequency of ceramic resonances on the ceramic radius.

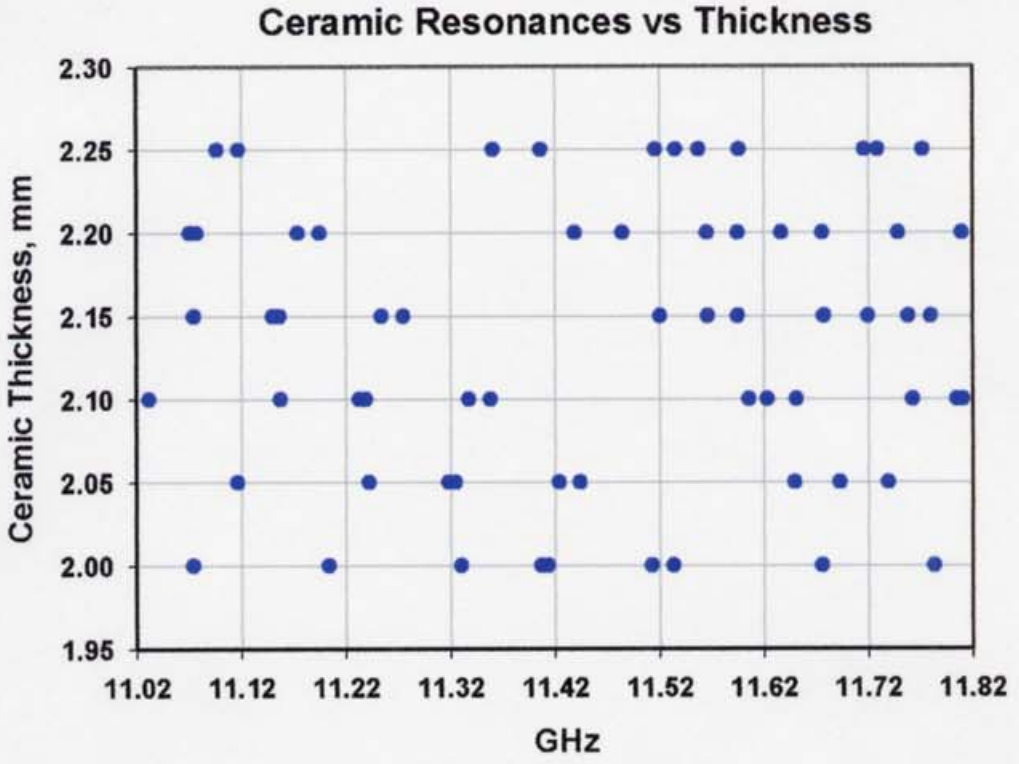

Figure 5.1.4: Dependence of the frequency of ceramic resonances on the ceramic thickness.

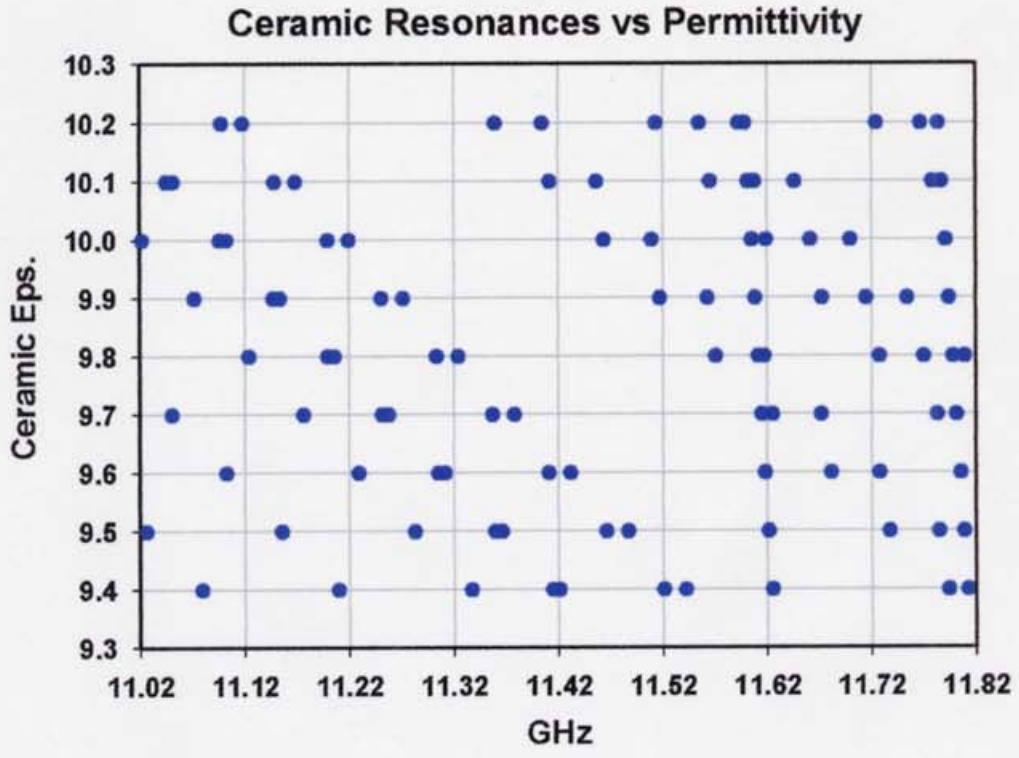

Figure 5.1.5: Dependence of the frequency of ceramic resonances on the ceramic permittivity.

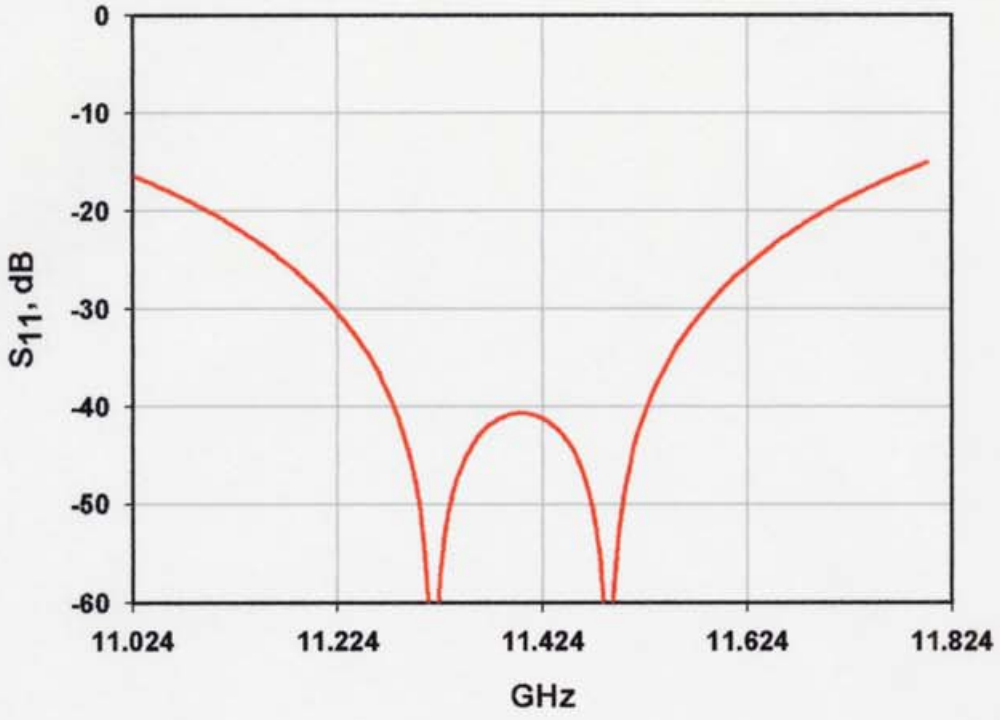

Figure 5.1.6: Passband of X-band TE_{01}-TE_{02} travelling-wave window.

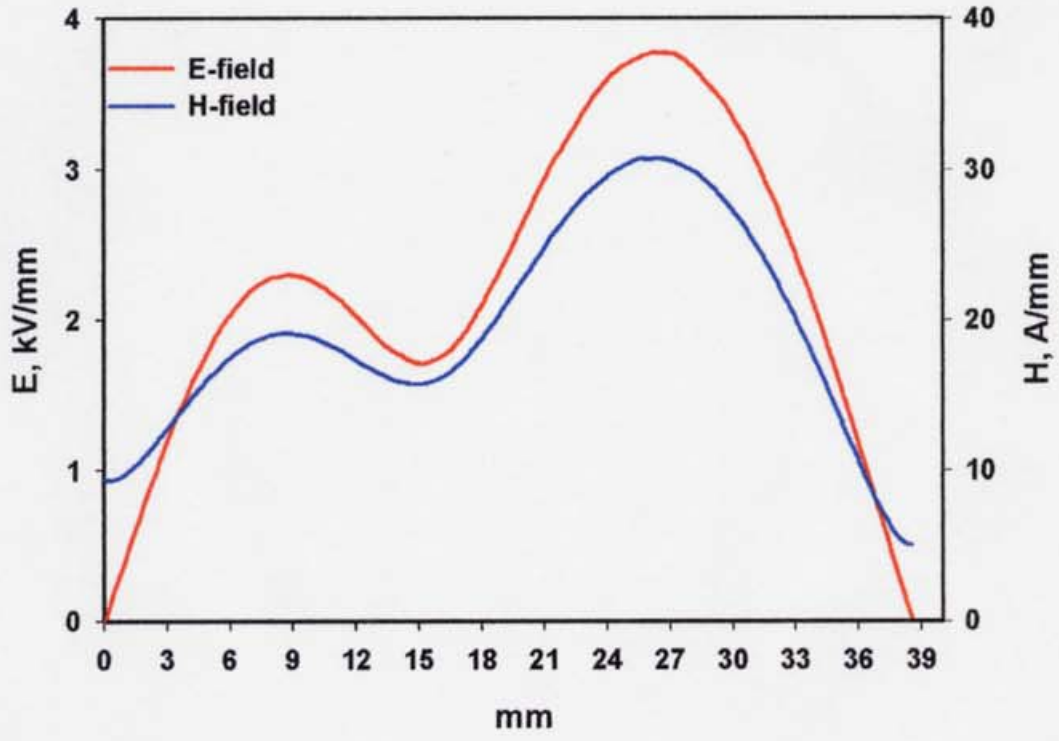

Figure 5.1.7: Electric and magnetic fields on the ceramic surface of X-band TE_{01}-TE_{02} travelling-wave window at power of 100 MW.

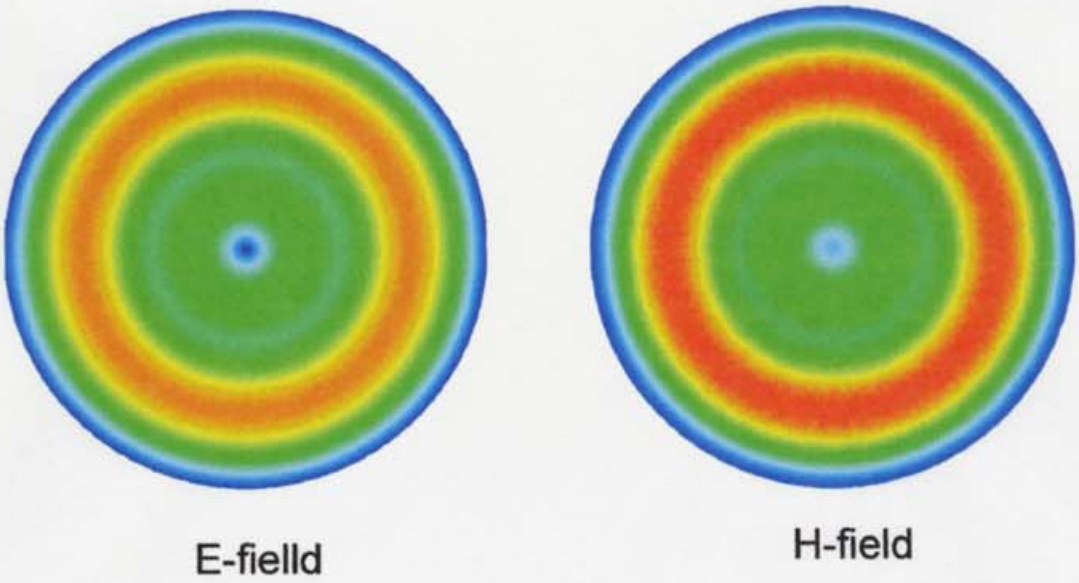

Figure 5.1.8: Electric and magnetic fields on the ceramic surface of X-band TE_{01}-TE_{02} travelling-wave window.

5.2 New TE_{10}-TE_{01} mode converter

We have designed several different TE_{10}-TE_{01} mode converters for JLC project. Pictures of some of them can be found in Appendix 6. Here, we would like to describe the development of the last one in detail. It is our opinion that it is more suitable for TE_{01}-windows. The geometry of converter and its main sizes are given in Fig. 5.2.1. Simulations show that the converter has 240 MHz passband where the efficiency of conversion is more than 99%. The efficiency at the operating frequency is 99.99%. Figure 5.2.2 shows the passband of converter. Figures 5.2.3 and 5.2.4 show the electric and magnetic fields on the converter surface for 100 MW power respectively. The parameters of converters are summarized in Table 5.2.1

Table 5.2.1: Parameters of TE_{10}-TE_{01} mode converter.

Operating frequency	11424 MHz
Modes to convert	$TE_{10} \leftrightarrow TE_{01}$
Efficiency of conversion	99.99%
Passband (Eff. > 99%)	240 MHz
Max. E-field on the surface (at 100 MW)	46 kV/mm

The principle of conversion is not obvious from its converter shape. It will be useful to give brief quality description of the working principle. Suppose we have the connection between rectangular and circular waveguides. Suppose also that we have the TE_{02} mode in the rectangular waveguiade. If the diameter of circular waveguide meets the conditions that $1.22\lambda_0 < D < 1.64\lambda_0$, only two TE_{21} and TE_{01} modes are generated in the circular waveguide, see Fig. 5.2.5. The TE_{21} and TE_{01} modes are not coupled in the circular waveguide. But if we put a perturbance, which satisfies both TE_{21} and TE_{01} symmetry conditions, the modes get coupled and can be converted from one to another, see Fig. 5.2.6. If we now combine the first and second parts right way, it is possible to have a TE_{20}-TE_{01} mode converter, see Fig. 5.2.7. The TE_{10} mode can be transformed to TE_{20} mode by a junction of rectangular waveguides, see Fig. 5.2.8. Combination of all parts gives the TE_{10}-TE_{02} mode converter, see Fig. 5.2.9.

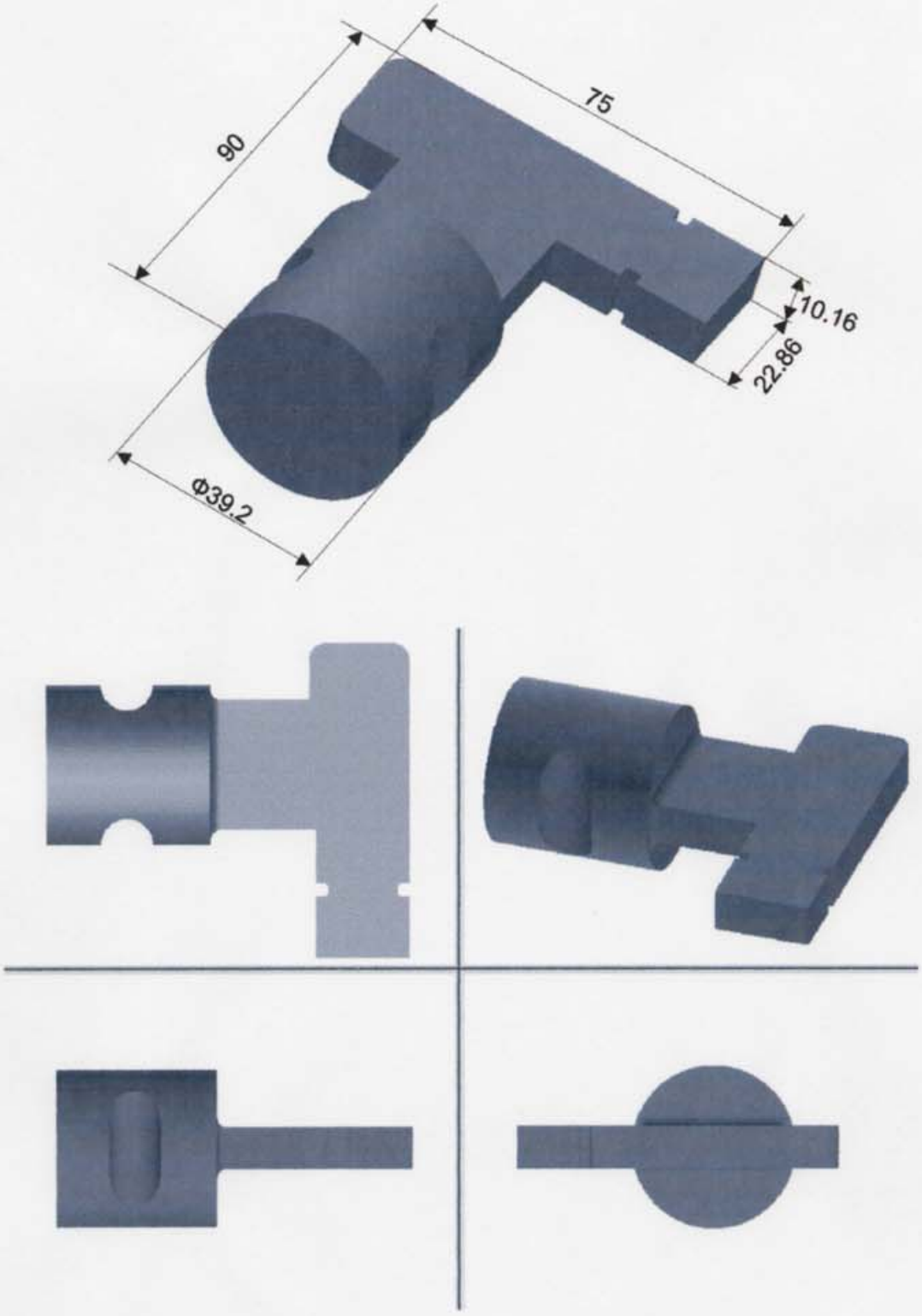

Figure 5.2.1: Geometry of the new X-band TE_{10}-TE_{01} mode converter.

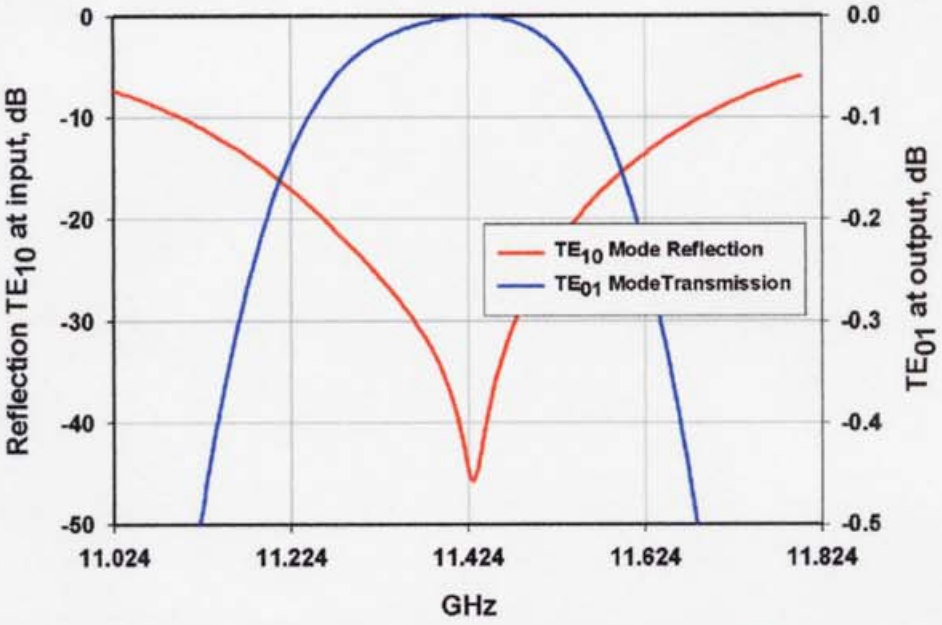

Figure 5.2.2: Passband of the new X-band mode converter

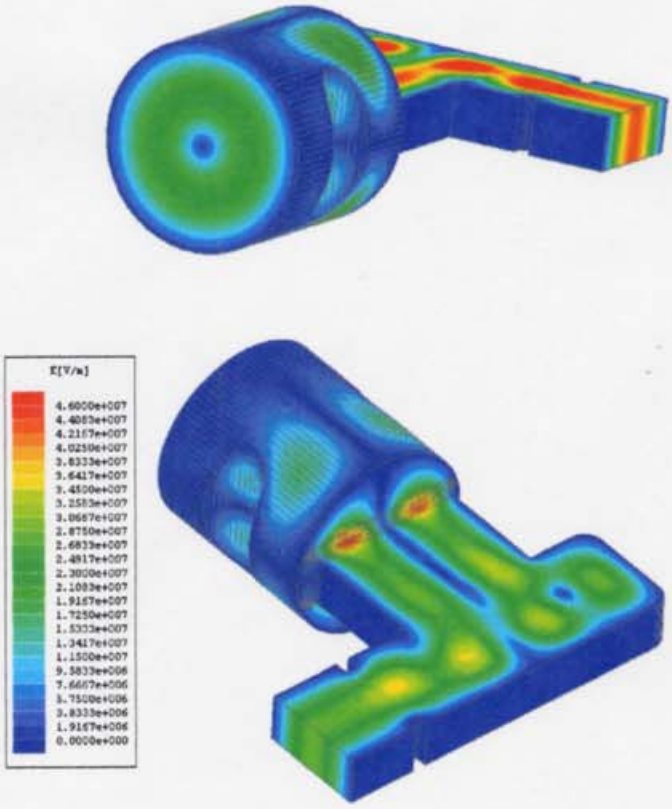

Figure 5.2.3: Electric field on the surface of new X-band mode converters at power of 100 MW.

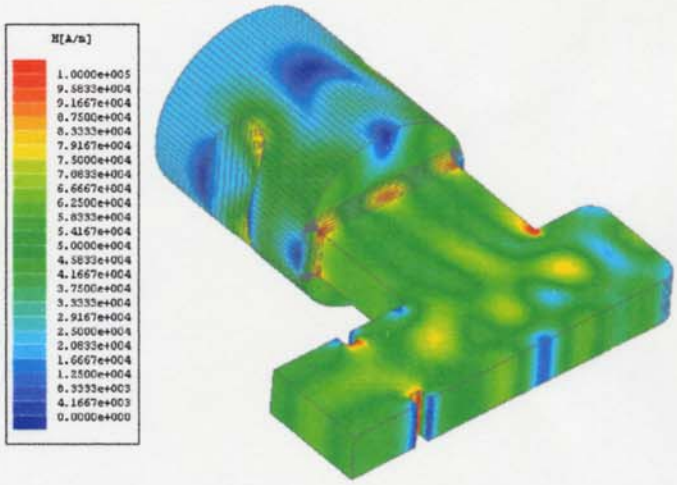

Figure 5.2.4: Magnetic field on the surface of the new X-band mode converters at power of 100 MW.

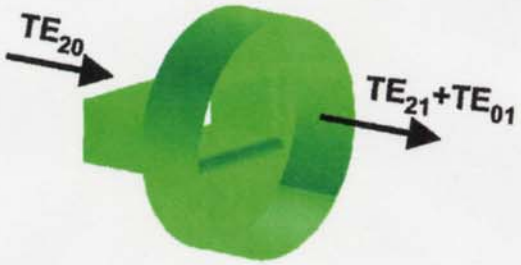

Figure 5.2.5: TE_{20} modes generate only TE_{21} and TE_{01} modes.

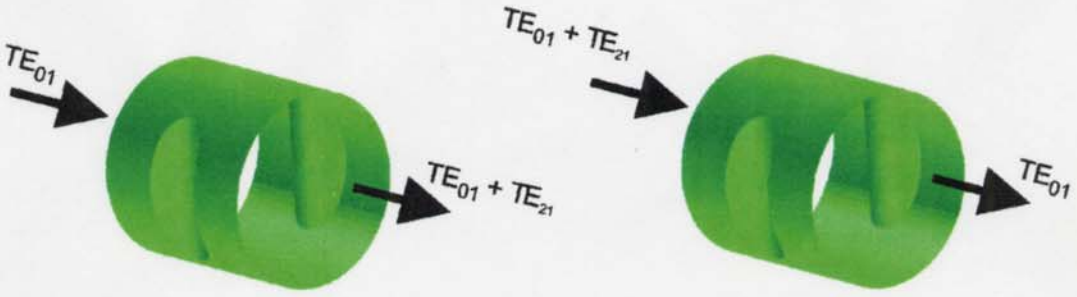

Figure 5.2.6: Perturbance couples TE_{21} and TE_{01} modes.

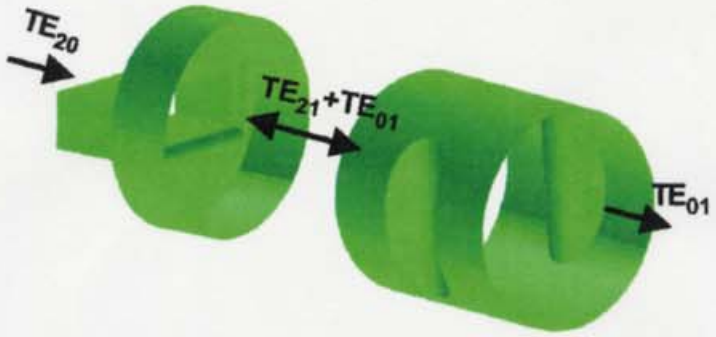

Figure 5.2.7: Combination of two parts realizes a TE_{20}-TE_{01} mode converter.

Figure 5.2.8: Junction of rectangular waveguides transforms TE_{10} mode to TE_{20} mode.

Figure 5.2.9: All parts together compose a TE_{10}-TE_{01} mode converter.

5.3 Test of TE01-TE02 travelling-wave window at low power level

To check the simulation and to make the final adjustment, the models of window and two converters were made and low-power measurements were carried out. The several antennas were built in the cylindrical part of window. Some antennas were placed near the ceramic to measure ghost modes, and some were placed far from the ceramic to measure volume resonances. Figures 5.3.1 – 5.3.6 show the hardware parts for low power measurements.

First of all, the SWR of the window and the converters were measured using a matched load. The measurements have some complexity because the mode converter is always present at measurements. We should separate the characteristics of the window and the converter, or the converter and the load, if the load is not ideal. For this purpose, the method of "sliding loads" was used. The main point of method is several measurements for different distances between two objects. If the reflection of each object is small enough (it is true in our case), the point of joint reflection makes a circle on the complex plane. The center of circle corresponds to the reflection of the object nearest to the RF source; the radius of circle is equal to the magnitude of the second object reflection. As example, Fig. 5.3.7 shows the reflection of load for different positions of matching iris.

The passbands of two converters are presented in Fig. 5.3.8. The window was measured for different cylindrical parts. The result shows that best SWR corresponds to the cylinder length longer than the calculated one by 0.4mm. Window passband is shown in Fig. 5.3.9. Window resonances were measured through the antennas. The two types of antennas were used – pins and loops. During these measurements, the converters were disconnected from the window, and the pipes of window were open (radiating in air). From plots in Figs. 5.3.10 and 5.3.11, we can see that the window has no resonances near the operating frequency.

After the full assembly, the window with two converters was measured. The goal was to find distances between the window and the converters to provide good SWR and no resonances around the operating frequency. The distance between the window and the converters was changed by a set of spacers from 0 to 32 mm with 2 mm step. Resonances were observed through the antennas. However it turned out that we could see all resonances on the SWR curve. The optimal distances for orthogonal and parallel positions of converters were found. The orthogonal position has slightly lower density of resonances and more sets of distances, which meets window requirements. Figures 5.3.12 and 5.3.13 show examples of

SWR at the full window assembly for the orthogonal and parallel converter position, respectively.

Figure 5.3.1: Low power elements: two converters, window, load, spacers.

Figure 5.3.3: Converter, window, and load.

Figure 5.3.2: Ceramic unit with antennas.

Figure 5.3.4: Converter.

Figure 5.3.5: Window together with two converters. Orthogonal position.

Figure 5.3.6: Window together with two converters. Parallel position

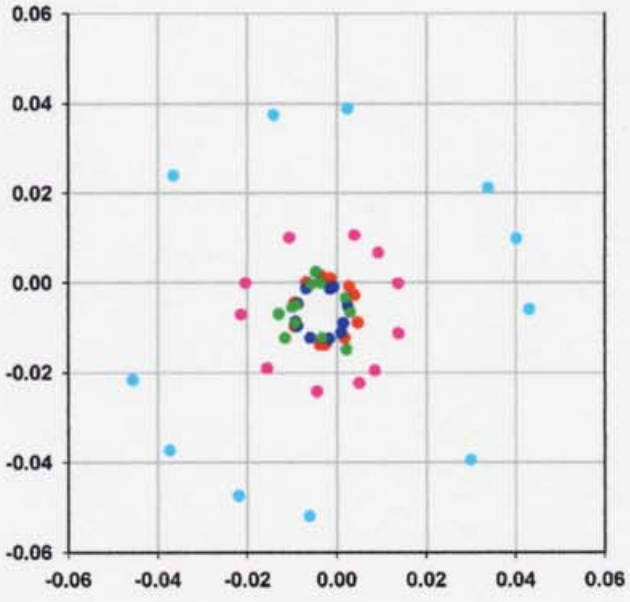

Figure 5.3.7: "Sliding Load" method. Reflection of load at different positions of different matching irises.

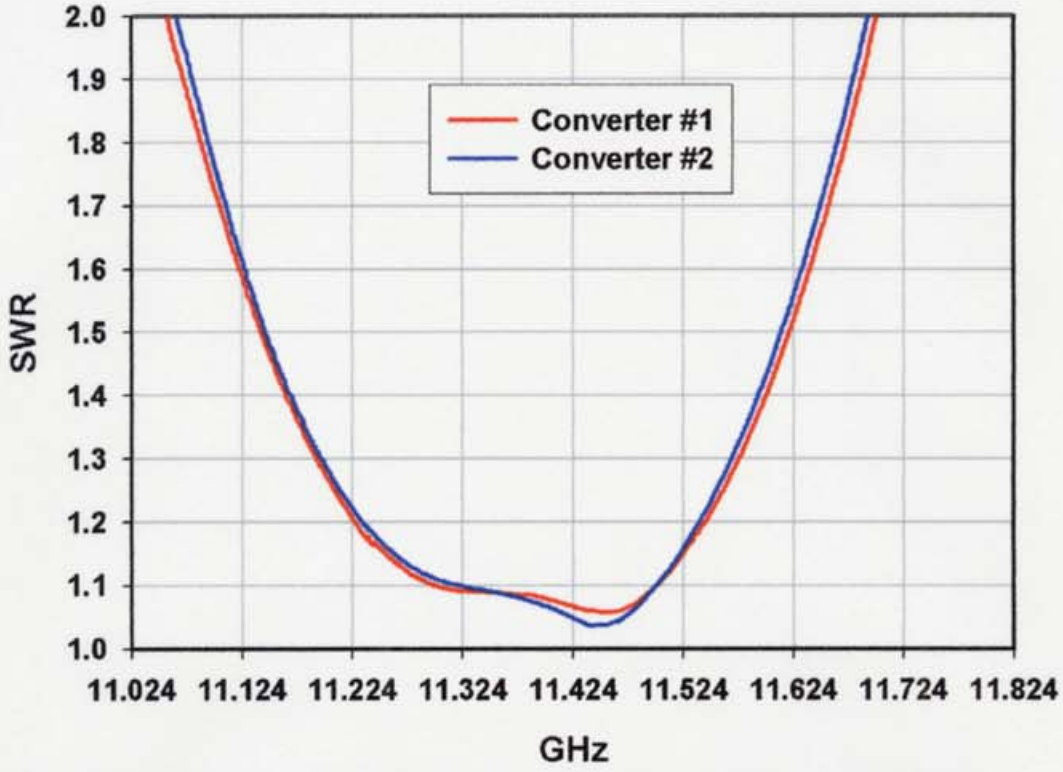

Figure 5.3.8: Passbands of the new X-band TE_{10}-TE_{01}mode converters.

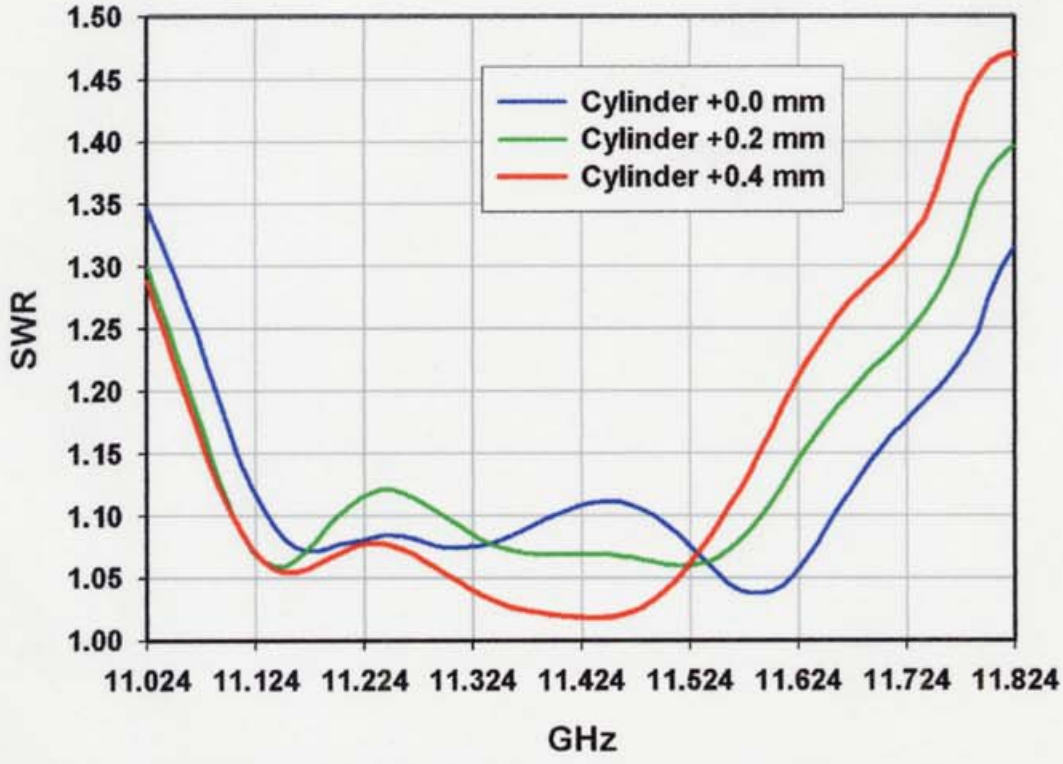

Figure 5.3.9: Passband of TE_{01}-TE_{02} travelling –wave window with different cylindrical parts.

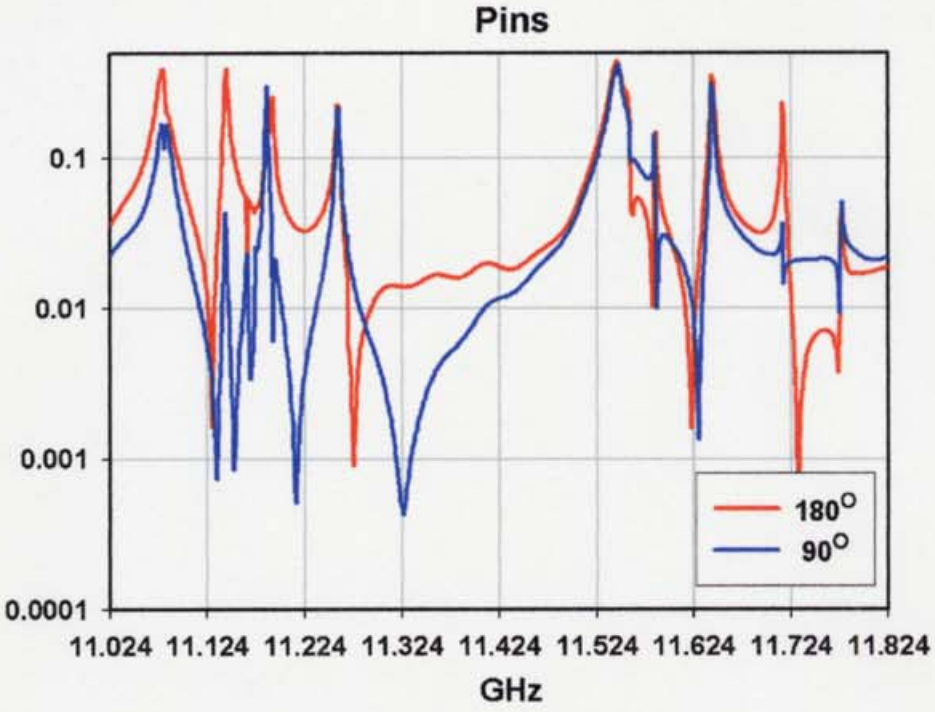

Figure 5.3.10: TE_{01}-TE_{02} Travelling-wave window resonances measured by pins. Pins positions are 180^{O} and 90^{O} to each other.

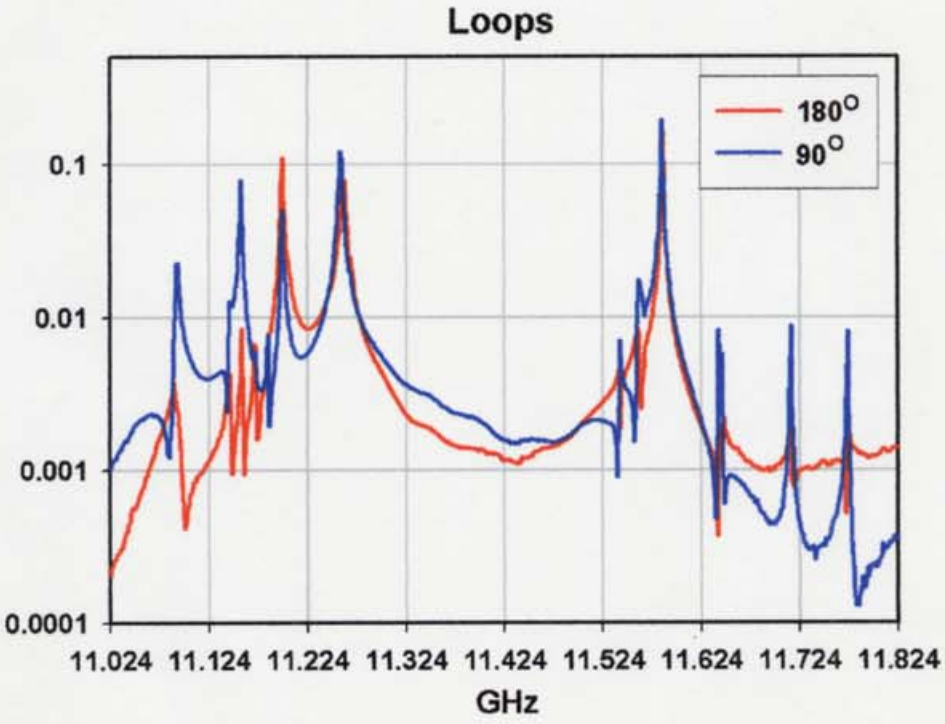

Figure 5.3.11: TE_{01}-TE_{02} travelling-wave window resonances measured by loops. Loops positions are 180^{O} and 90^{O} to each other.

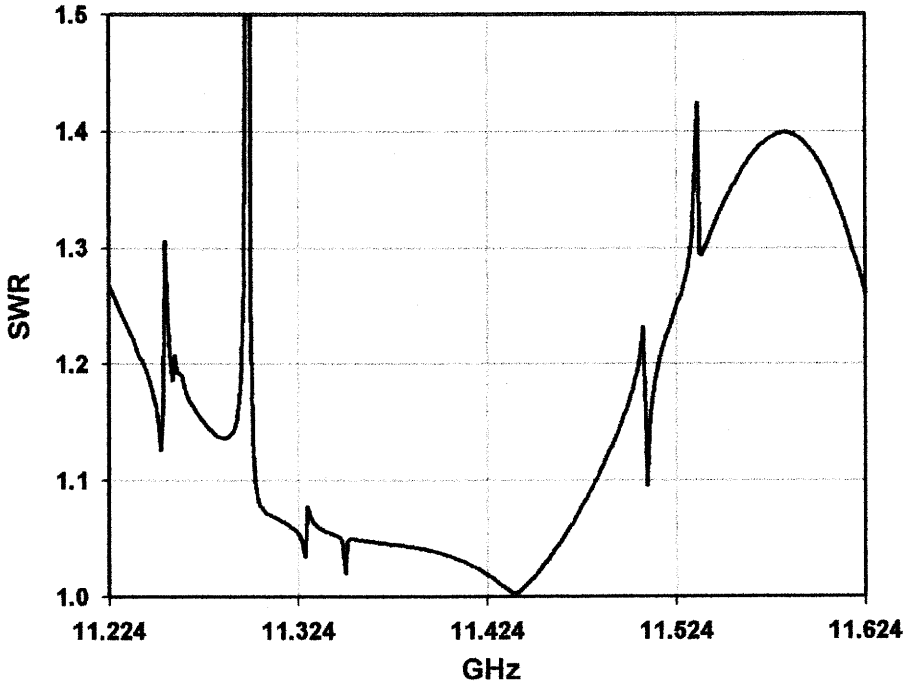

Figure 5.3.12: Passband of TE_{01}-TE_{02} travelling- wave window with two mode converters. The converter position is orthogonal.

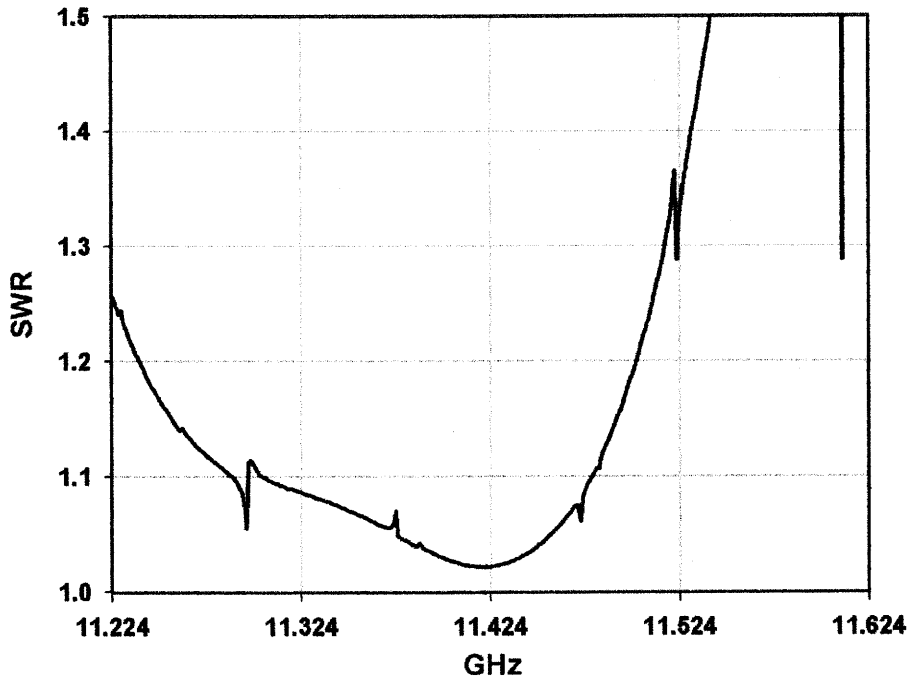

Figure 5.3.13: Passband of TE_{01}-TE_{02} travelling-wave window with two mode converters. The converter position is parallel.

5.4 Summary

The X-band (11424 MHz) oversized window with travelling-wave in ceramic and the combinations of TE_{01} and TE_{02} modes on the surface was designed. The window has the maximum electric field on the ceramic of 3.77 kV/mm for 100 MW power. There is no electric field at the ceramic-metal brazing area. The new type of TE_{10}-TE_{01} mode converter is designed. The converter is compact and simple for manufacturing. The low power models of the window and the converters were made. The measurements confirmed the calculations. The whole geometry of the window with the converters was found to have good SWR and to be free from resonances near the operating frequency.

Chapter 6
Conclusions and summary

In conclusions we can say that the goals formulated at the beginning of the thesis are achieved:

Travelling-wave window concept

The concept of window with travelling-wave in ceramic (TW window) was proposed. **It allows to reduce the electric field on the ceramic by about factor of two** in comparison with half-wave windows. **The new type of window has a larger passband** than half-wave one. The optimum of the ceramic thickness is a quarter of wavelength, twice smaller than the half-wave window. **It reduces the density of ghost modes and allows to increase a ceramic size.**

Travelling-wave S-band test window

To check the TW window concept, the S-band window was designed and manufactured. The window was tested by the resonant ring and showed excellent performances. **The power 470 MW at 2μs at 50 pps was transmitted through the window without being destroyed** and it still kept vacuum tightness. We believe, this is the best result for S-band windows up to date.

X-band travelling-wave mixed mode window

The weakest point of window is the ceramic-metal brazing place. The new type of TW X-band window was developed. The field on the ceramic is the combination of several modes, and the electric fields strength is rather small at the periphery. At the same time, the window is simple, compact and wideband. The window was high-power tested. **The power 100 MW at 0.5 μs and 85 MW at 1.5 μs was transmitted through the window successfully. Now this type of window is used in the 75 MW E3761 Toshiba klystrons.**

X-band TE01-TE02 travelling-wave window

To achieve a complete reliability we need a window which can stand four times more power than RF sources has one. For this purpose the oversize X-band TW window with ceramic diameter of 77.1 mm was designed. The field in the ceramic area is the mixture of two TE_{01} and TE_{02} modes. It provides **zero electric field in ceramic-metal brazing place**. The window has advantages of simple geometry, wideband and low electric field on the ceramic: **3.77 kV/mm at 100 MW power. It gives a hope that window will be able to transmit several hundreds of MW.**

The new, simple and effective TE_{10}-TE_{01} mode converter was designed for this window. The low power models of the window and the converters were made and measured. The geometry with good SWR, passband but without resonances near the operating frequency was found.

Table 6.1.1: Developed windows

Table 6.1.2: Developed TE_{10}-TE_{01} mode converter

Oper. frequency, MHz		11424	
Efficiency, %		99.99	**TE_{01}-TE_{02} TW window**
Passband, MHz (Eff > 99%)		240	
Max. E on the surface, kV/mm (100 MW) MHz		46	11424
Pass band MHz (SWR<1.2)	100	440	600
Ceramic diameter, mm	84.2	53	77.1
Ceramic thickness, mm	7.59	2	2.12
Max. E on ceramic, kV/mm, (100 MW)	3.1	7.8	3.77
Max. E at ceramic-metal, kV/mm, (100 MW)	2.0	0.44	0
Max. E at metal, kV/mm, (100 MW)	18	52	0
Test	470MW / 2μs / 50 pps	100MW / 0.5μs 85MW / 1.5μs / 30 pps	--

Acknowledgments

First of all, I would like to express my special gratitude to Professors H.Mizuno and K.Takata. The works presented in this thesis could not have started without their interest and continuous support.

I am very grateful to Professor Y.H.Chin for the opportunity to continue this work in a perfect creative atmosphere of KEK and for hard labor of the first reading of this thesis.

I wish to thank Dr. Y.Saito and Dr. S. Michizono for the great help with the tests of the S-band window.

I would like to thank Dr. S.Tokumoto, Dr. Y.Otake, Dr. S.Yamaguchi, Dr. S.Matsumoto and the SLAC team for testing of the X-band windows.

I would like to thank Dr. A.Lunin for his assistace for some cold measurements.

And at last, I wish to thank the staff of BINP (Protvino) for manufacturing the S-band window.

Appendix 1

Ghost modes in circular waveguide with dielectric disk.

Denotations:

k_{0x} - wave vector of plane wave in infinite media x

$k_{0x} = \omega\sqrt{\varepsilon_x \mu_x}$

ε_x, μ_x - permittivity and magnetic permeability of media x

$k_\perp$ - transverse wave vector. In case of circular waveguide $k_\perp = \frac{A_{nm}}{R}$

A_{nm} - mth-root of equation $J_n(A_{nm}) = 0$ for TM modes and $J_n'(A_{nm}) = 0$ for TE modes

G_x - longitudinal wave vector; $G_x^2 = k_{0x}^2 - k_\perp^2$

$Z_{0x} = \sqrt{\frac{\mu_x}{\varepsilon_x}}$ - wave impedance of media x

Z_x - wave impedance of mode in waveguide filled by media x

$Z_x = Z_{0x}\frac{G_x}{k_{0x}}$ for TM mode; $Z_x = Z_{0x}\frac{k_{0x}}{G_x}$ for TE mode

Suppose that the disk of media 2 is placed in a circular waveguide filled by the media 1 and $\varepsilon_2\mu_2 > \varepsilon_1\mu_1$, see Figure A1.1.

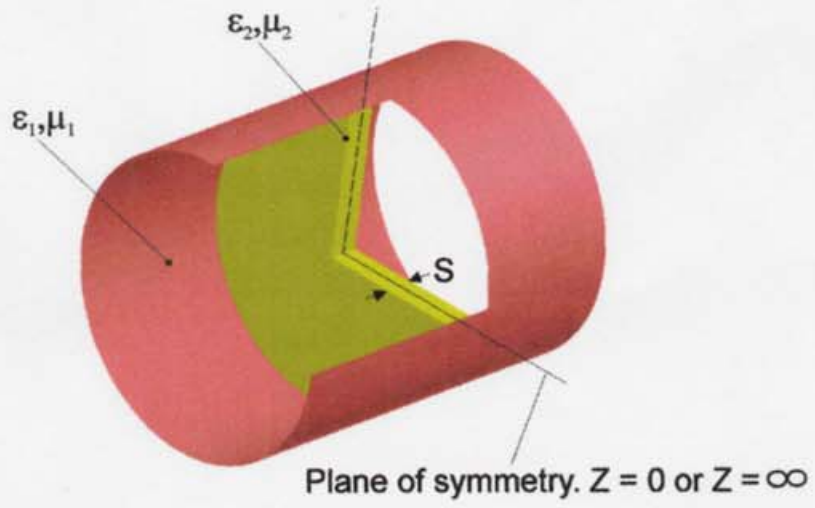

Figure A1.1: Dielectric in circular waveguide

The disk thickness is S. There exists ω which satisfied that $G_1^2 < 0$ and $G_2^2 > 0$. It means that G_1 is pure imaginary and the wave does not propagate in waveguide part 1. The vector G_2 is real and the wave propagates in disk without attenuation. The wave is completely reflected from the media boundary and there are resonance conditions for some combinations of frequency and disk sizes. Let us write down the equations, which connected the frequency with other parameters.

From the symmetry, resonance solutions satisfy the boundary condition of E- or H- wall in the middle of the disk. It means that the solution has impedance 0 or ∞ in the middle of the disk. To satisfy boundary condition, the impedance at the boundary of medias must be equal to Z_1. Knowing impedance in one plane, we can recalculate in another one and equate it to required one.

The zero impedance in middle plane corresponds $-iZ_2 tg(G_2 \frac{S}{2})$ in plane of media boundary. At the same time, it must be equal to $Z_{01}\frac{G_1}{k_{01}}$ for TM mode and $Z_{01}\frac{k_{01}}{G_1}$ for TE mode. We have two equations:

$$-iZ_{02}\frac{G_2}{k_{02}} tg(G_2 \frac{S}{2}) = Z_{01}\frac{G_1}{k_{01}}$$

and

$$-iZ_{02}\frac{k_{02}}{G_2} tg(G_2 \frac{S}{2}) = Z_{01}\frac{k_{01}}{G_1}$$

Other couple equations that we have for ∞ impedance in the middle are:

$$iZ_{02}\frac{G_2}{k_{02}} ctg(G_2 \frac{S}{2}) = Z_{01}\frac{G_1}{k_{01}}$$

and

$$iZ_{02}\frac{k_{02}}{G_2} ctg(G_2 \frac{S}{2}) = Z_{01}\frac{k_{01}}{G_1}$$

Writing these equations in detail, we have:

$$tg\left(\frac{S}{2}\sqrt{\omega^2\varepsilon_2\mu_2 - \frac{A_{nm}^2}{R^2}}\right) = -\frac{\varepsilon_2\sqrt{\frac{A_{nm}^2}{R^2} - \omega^2\varepsilon_1\mu_1}}{\varepsilon_1\sqrt{\omega^2\varepsilon_2\mu_2 - \frac{A_{nm}^2}{R^2}}}$$

$$tg\left(\frac{S}{2}\sqrt{\omega^2\varepsilon_2\mu_2 - \frac{A_{nm}^2}{R^2}}\right) = \frac{\mu_1\sqrt{\omega^2\varepsilon_2\mu_2 - \frac{A_{nm}^2}{R^2}}}{\mu_2\sqrt{\frac{A_{nm}^2}{R^2} - \omega^2\varepsilon_1\mu_1}}$$

$$ctg\left(\frac{S}{2}\sqrt{\omega^2\varepsilon_2\mu_2-\frac{A_{nm}^2}{R^2}}\right)=\frac{\varepsilon_2\sqrt{\frac{A_{nm}^2}{R^2}-\omega^2\varepsilon_1\mu_1}}{\varepsilon_1\sqrt{\omega^2\varepsilon_2\mu_2-\frac{A_{nm}^2}{R^2}}}$$

$$ctg\left(\frac{S}{2}\sqrt{\omega^2\varepsilon_2\mu_2-\frac{A_{nm}^2}{R^2}}\right)=-\frac{\mu_1\sqrt{\omega^2\varepsilon_2\mu_2-\frac{A_{nm}^2}{R^2}}}{\mu_2\sqrt{\frac{A_{nm}^2}{R^2}-\omega^2\varepsilon_1\mu_1}}$$

By solving these equations, we can find the resonance frequencies ω.

Appendix 2
X-band pillbox window

This geometry pillbox window of this geometry was used in KEK klystrons XB50k and XB72k#1. The window was broken at power level of about 30 MW at 200 ns [8].

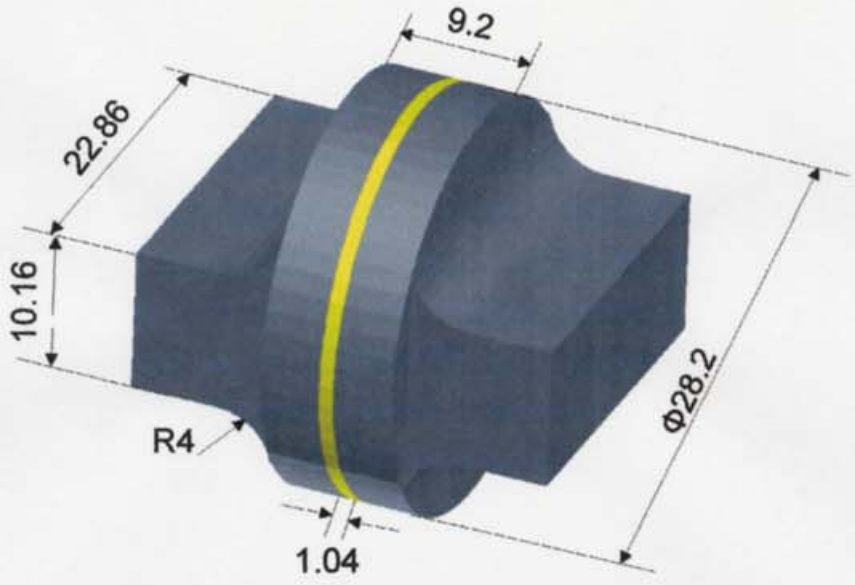

Figure A2.1: Geometry of X-band pillbox window

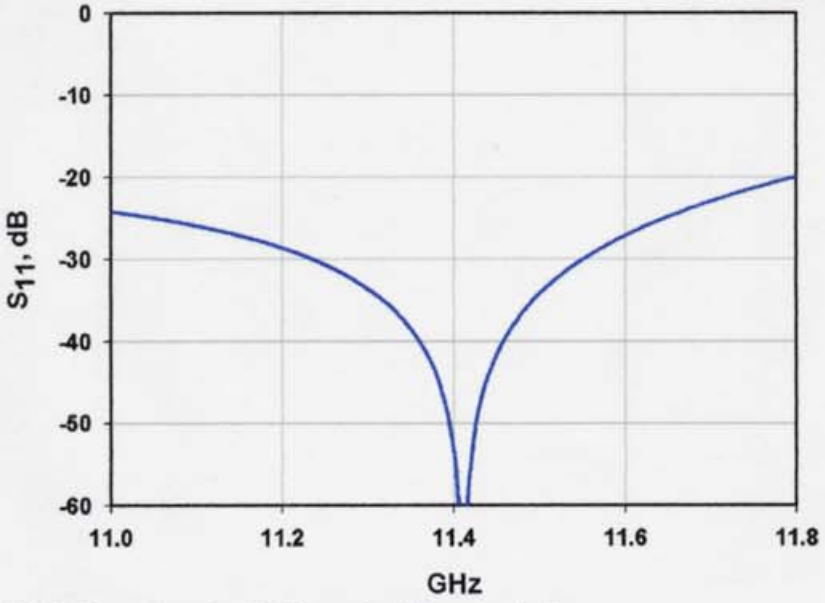

Figure A2.2: Passband of X-band pillbox window.

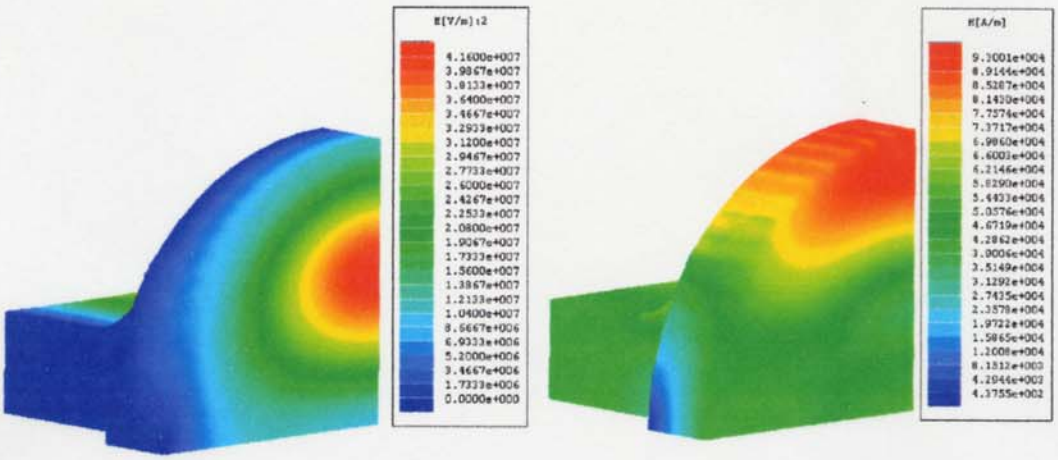

Electric field Magnetic field

Figure A2.3: Electric and magnetic fields on the ceramic surface of X-band pillbox window. Power kevel is 100 MW.

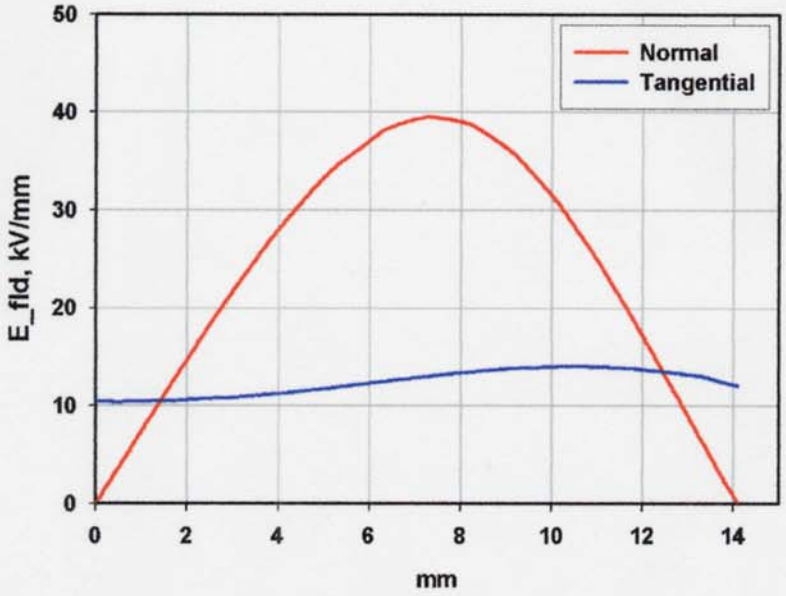

Figure A2.4: Electric fields on the ceramic surface. of X-band pillbox window. Power power level is 100 MW.

Appendix 3

X-band TE_{11}-mode window with taper transitions

The window was designed by Y.Otake at KEK. The window was tested usingthe resonant ring at power levels of 100 MW at 300 ns and 70 MW at 700 ns [11]. Window was used in several KEK-Toshiba X-band klystrons.

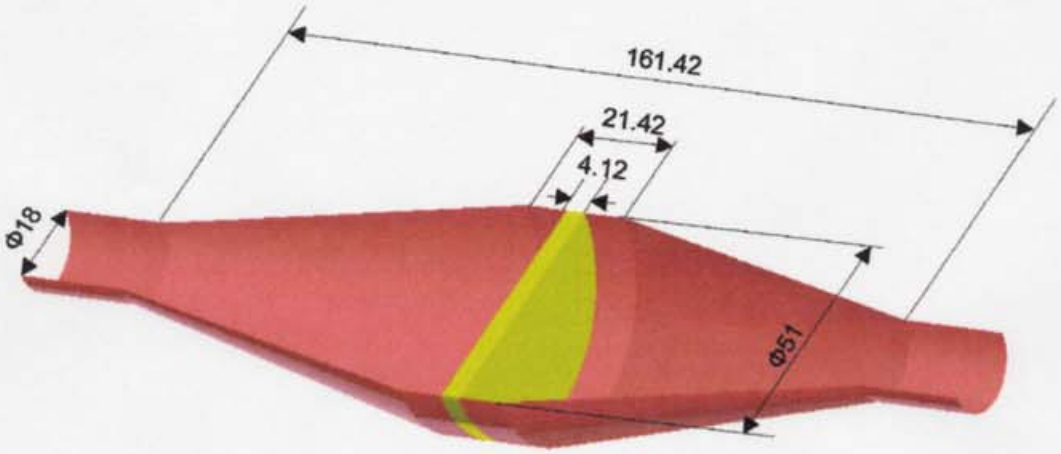

Figure A3.1: Geometry of X-band TE_{11}-mode window with taper transitions.

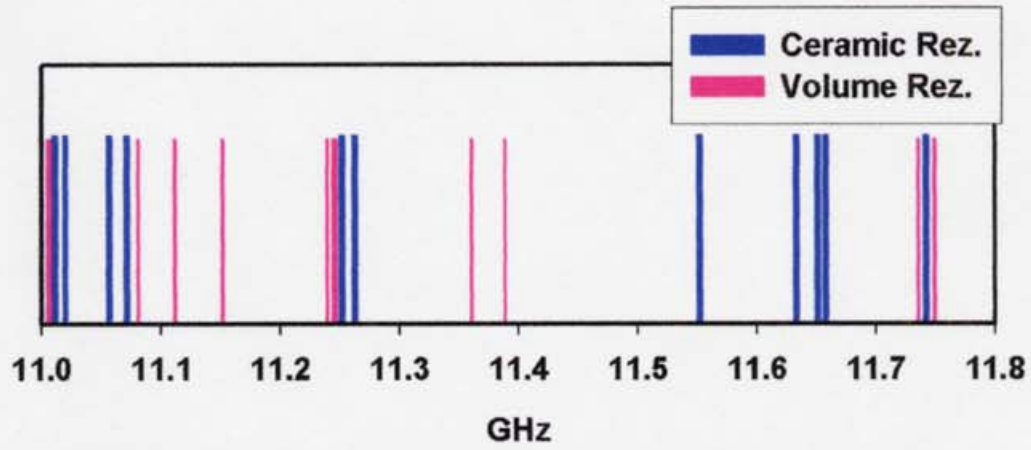

Figure A3.2: Resonances of X-band TE_{11}-mode window with taper transitions.

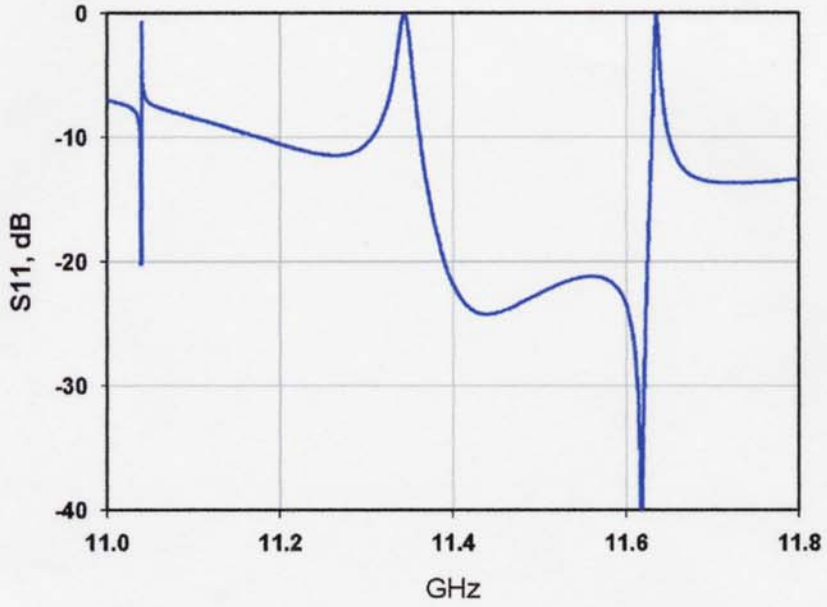

Figure A3.3: Passband of X-band TE_{11}-mode window with taper transitions.

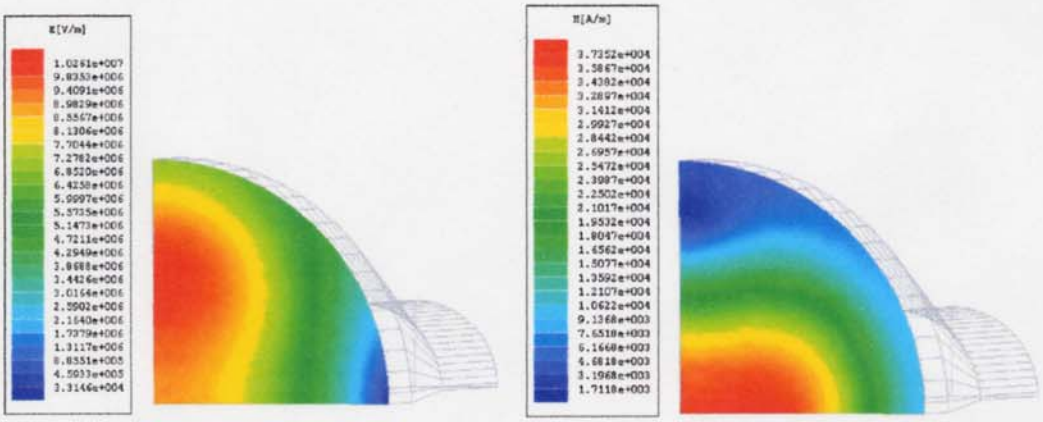

E-field H-field

Figure A3.4: Electric and Magnetic fields on the surface of ceramic of X-band TE_{11}-mode window with taper transitions. Power level is 100 MW.

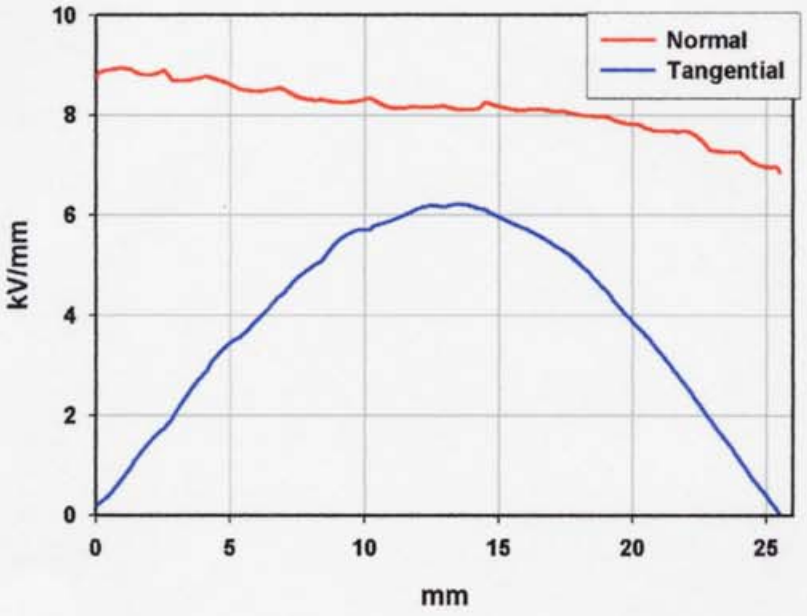

Figure A3.5: Electrical field on the on the surface of ceramic of X-band TE_{11}-mode window with taper transitions. Power level is 100 MW.

Appendix 4

65 mm TE_{01} X-band TW window designed at SLAC

The sizes of window for simulation were scaled from drawing []. The results can be different in some details from original, but the general properties, we think, are reproduced correctly. The window was tested at power level of 100 MW at 500 ns [15].

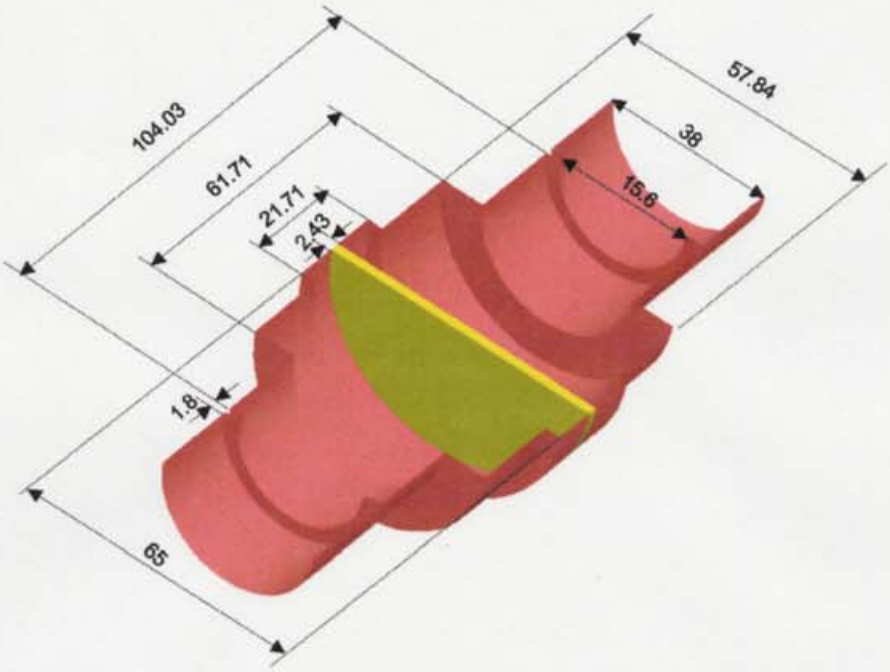

Figure A4.1: Geometry of 65 mm TE_{01} X-band TW window.

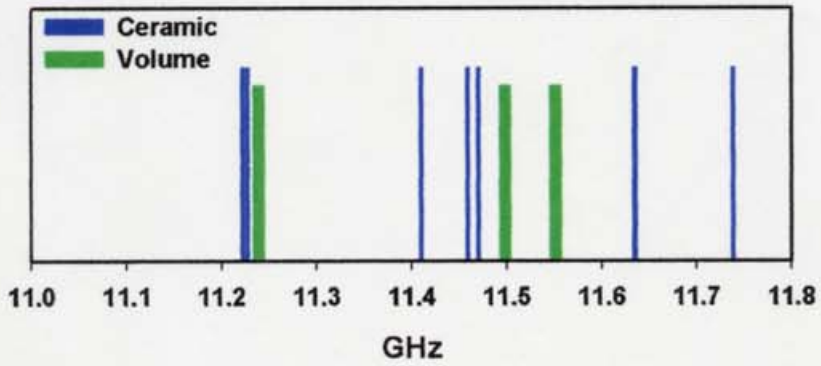

Figure A4.2: Resonances of 65 mm TE_{01} X-band TW window.

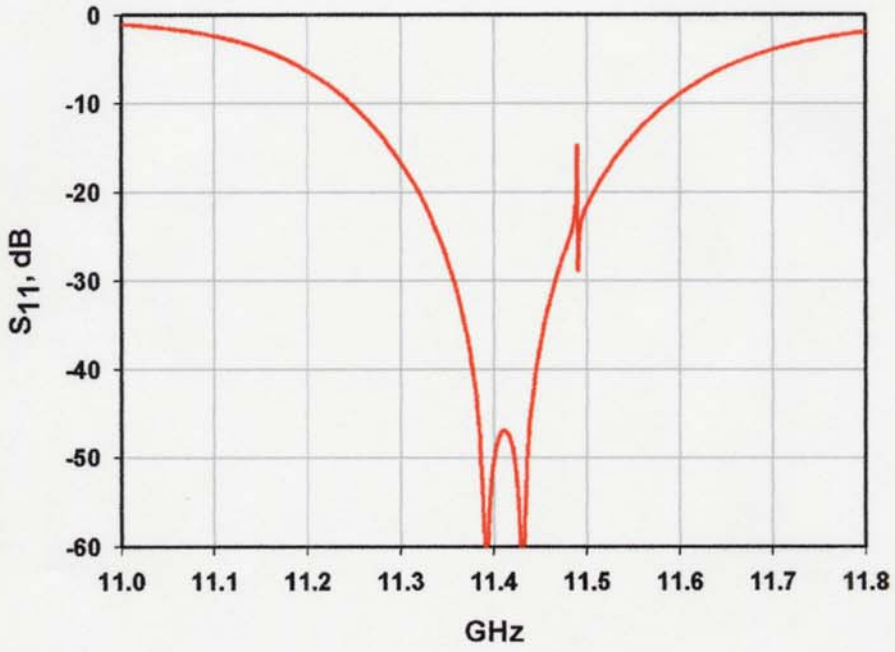

Figure A4.3: Passband of 65 mm TE_{01} X-band TW window.

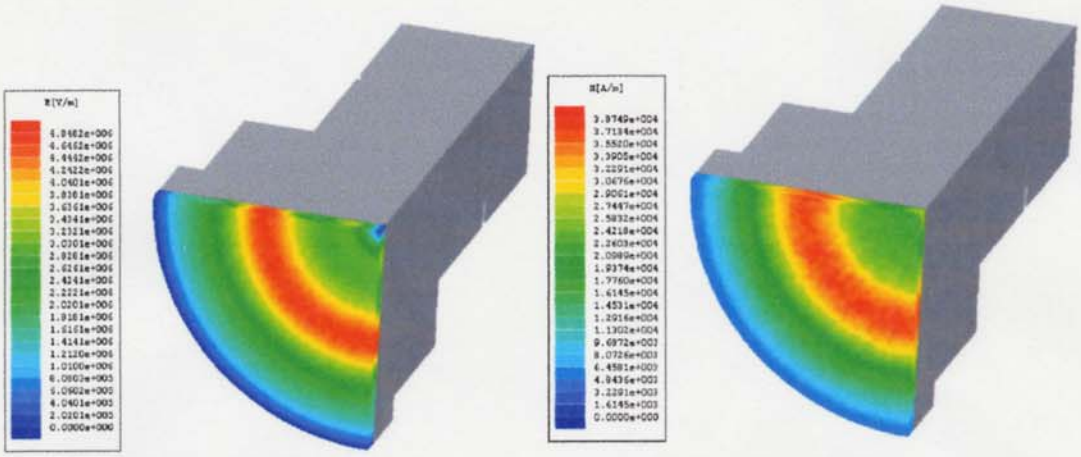

Figure A4.4: Electric and Magnetic field on the ceramic surface of 65 mm TE_{01} X-band TW window. Power level is 100 MW.

Appendix 5
Optimized geometry of X-band travelling-wave mixed-mode window

The geometry of X-band travelling wave mixed-mode window was optimized hands-off by computer. Valuation function took into account the passband and electric fields in the ceramic. Computer analyzed about 2000 options. In below, one of the best solution is presented.

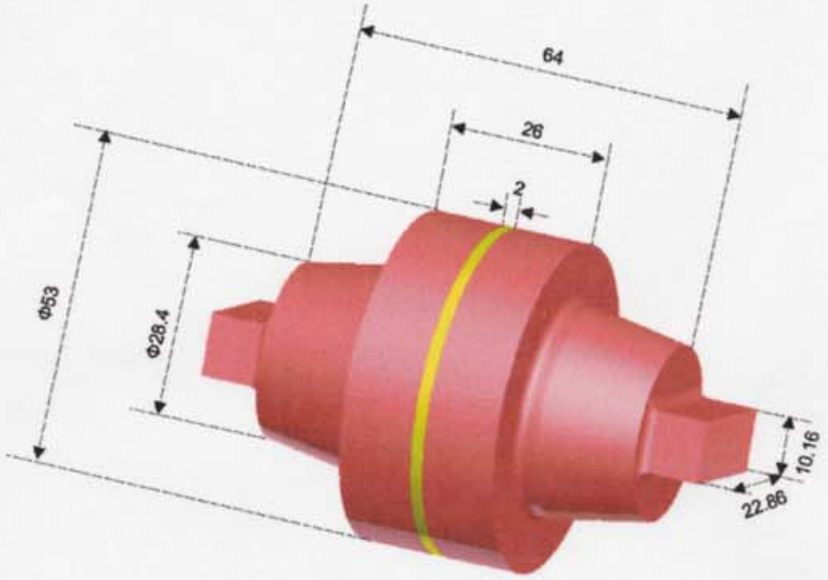

Figure A5.1: Main sizes of optimized geometry of X-band travelling wave mixed-mode window.

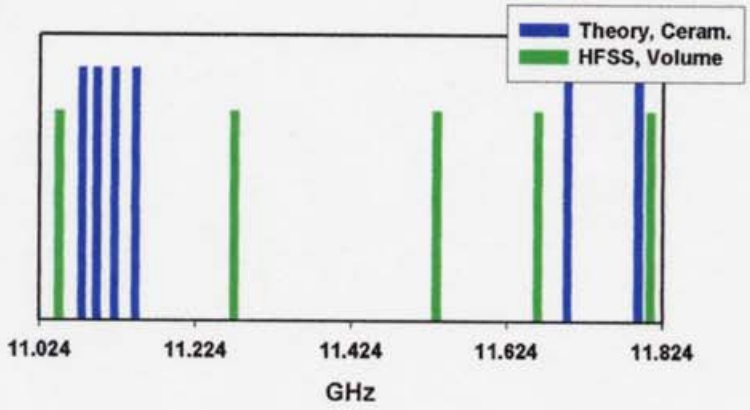

Figure A5.2: Resonances of X-band travelling wave mixed-mode window with optimized geometry.

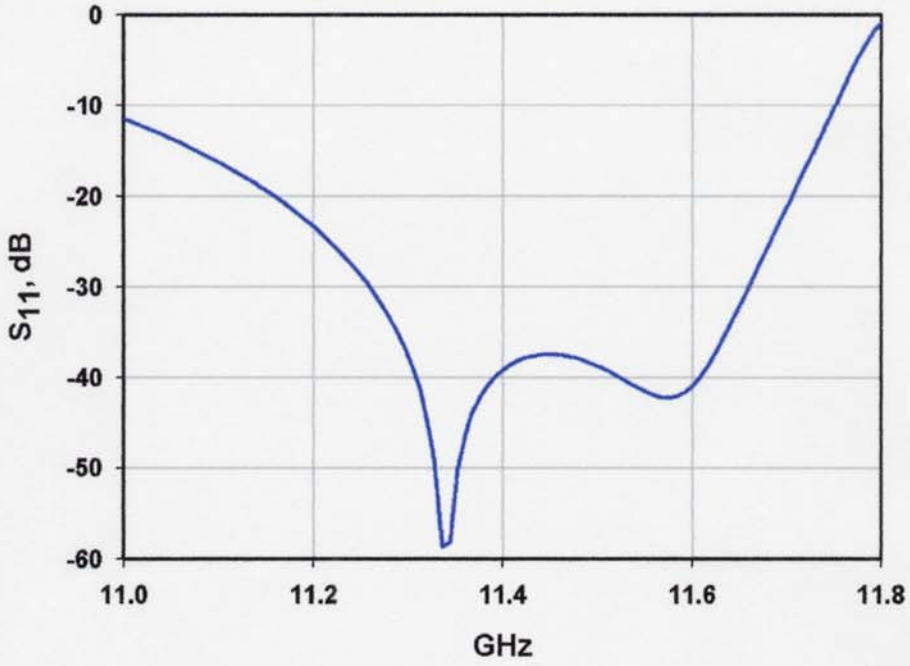

Figure A5.3: Passband of X-band travelling-wave mixed-mode window with optimized geometry.

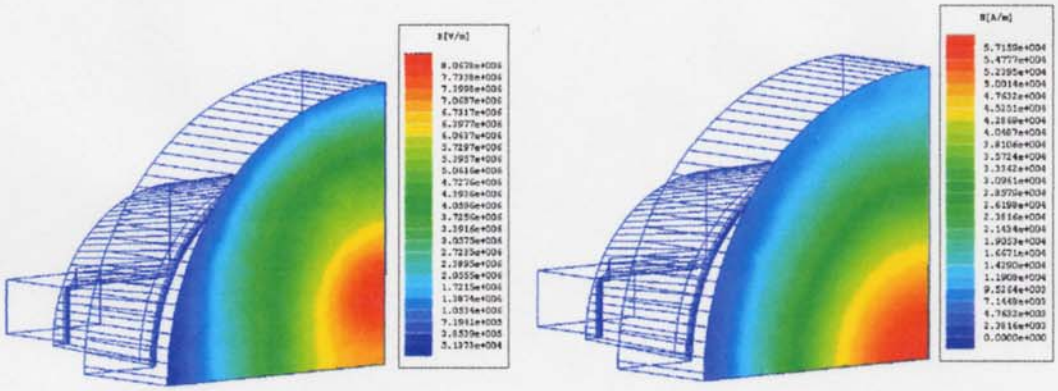

Figure A5.3: Electric and magnetic fields on the ceramic surface of X-band travelling-wave mixed-mode window with optimized geometry. Power level is 100 MW.

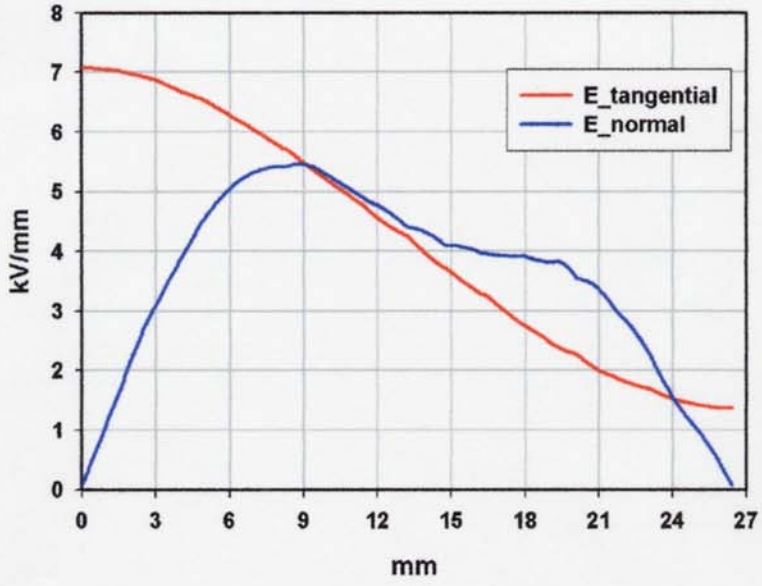

Figure A5.4: Electric field on the ceramic surface of X-band travelling-wave mixed-mode window with optimized geometry. Power level is 100 MW.

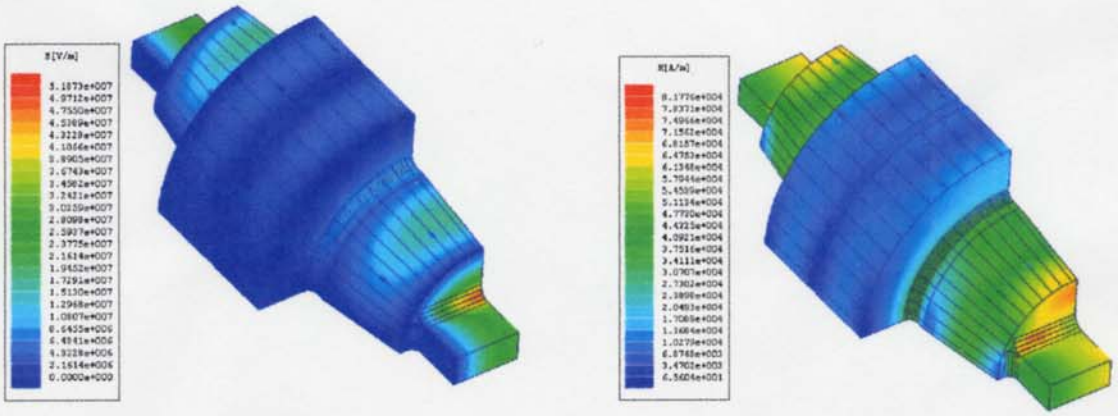

E-field H-field

Figure A5.5: Electric and magnetic fields on the metal surface of X-band travelling-wave mixed-mode window with optimized geometry. Power level is 100 MW.

Appendix 6

TE_{10}-TE_{01} mode converters designed for the JLC project

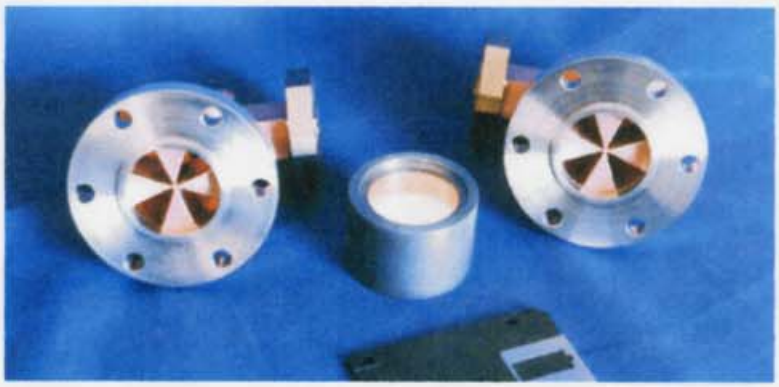

Figure A6.1: Cross TE_{10}-TE_{01} mode converter and window on its base.

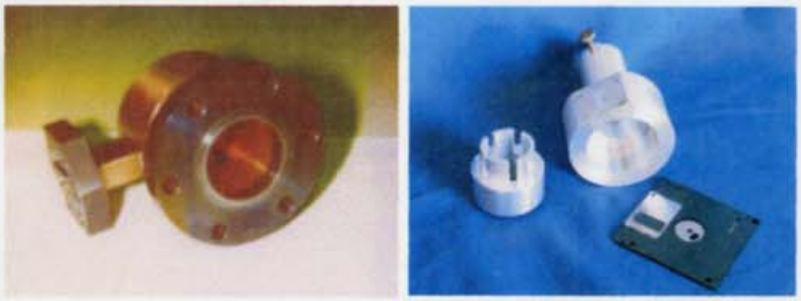

Figure A6.2: Wrap-around TE_{10}-TE_{01} mode converter

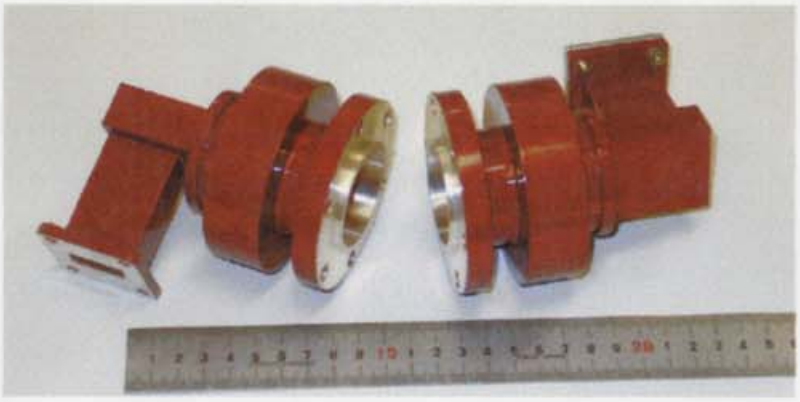

Figure A6.3: Choke TE_{10}-TE_{01} mode converter

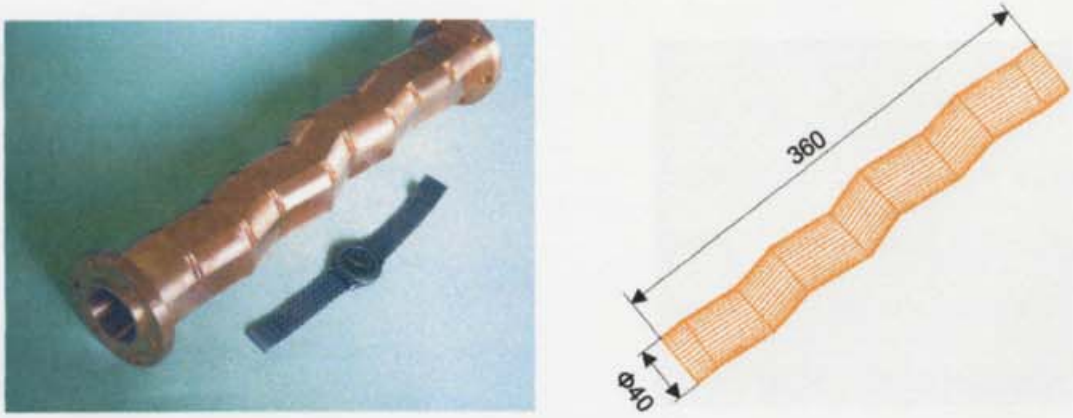

Figure A6.4: Zigzag TE_{11}-TE_{01} mode converter

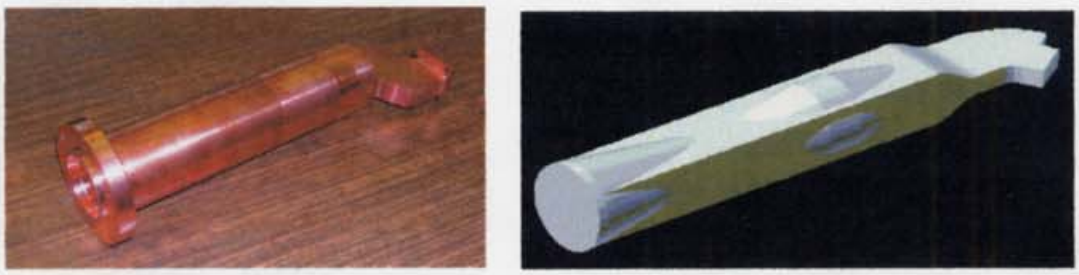

Figure A6.5: TE_{10}-TE_{01} converter-launcher

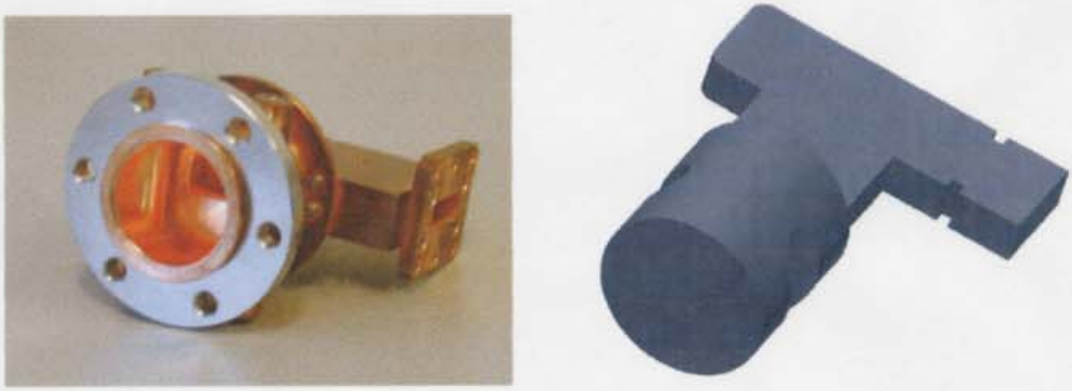

Figure A6.6: Iris TE_{10}-TE_{01} mode converter